國立成功大學
National Cheng Kung University

THESIS TITLE:

The Aerodynamics and Water Tunnel Testing of a Wingsuit

Fernando José De La Cruz Chávez (趙明宏)

Carlos Eduardo Banegas Flores (羅富亮)

Thesis supervisors:

張克勤 Chang, Keh-Chin

葉思沂 Yeh, Szu-I

周晉成 Zhou, Jin-Cheng

Index

1. Introduction

The latest facet and the next step in skydiving technology is wingsuit flight. Wingsuit flight gives the participant the exhilarating feeling of bird-like flight where the pilot can control his path through the sky in a wearable aircraft by physically changing the body position and shape. Wingsuit flight is an extreme sport, a particular form of skydiving, on which skilled skydivers and BASE jumpers wear a special suit that allow them to fly after jumping from a high altitude. This special suit called "Wingsuit" is designed to expand the body surface by creating wings under the arms and legs of the user in order to create more lift, making it possible to glide through the air by traveling longer distances horizontally. Unlike normal skydiving, where the fall is near vertically at approximately 45 m/s to 70 m/s, on the sport of wingsuit flying pilots generally achieve vertical (downward) descent velocities between 13 to 29 m/s and horizontal (forward) speeds of 20 to 70 m/s. [6] With current wingsuit designs it is not possible to land using just the wingsuit itself, instead the wingsuit pilot deploys a parachute at a safe altitude to descend to the ground.

Whether the pilot jumps from an airplane or from a B.A.S.E. (Building, Antenna, Span and Earth), by wearing a wingsuit he/she can jump into a steady glide usually reaching glide ratios of over 2:1, depending on the design of the wingsuit, which ends when the pilot opens the parachute. The glide ratio is the ratio between the lift force and the drag force, which is one of the most important parameters taken into account for the design of a wingsuit and it is usually preferred to be a high ratio in order to reach a long range flight.

1.1. Wingsuit history

The history of wingsuit flying dates back to 1912 when French tailor Franz Reichelt made the first attempt in a self-hand-sewn "parachute suit" by jumping from the first platform of the Eiffel Tower, falling 200 ft. straight to his death. After this, wingsuits have been developed and used not only in extreme sports, but also for military purposes.

During the 1930s, more daredevils and stuntmen started to design and build their own experimental wingsuits attempting to fulfill the dream of human flight, unfortunately most of them ended up with fatal results. It was not until the 1990s that the first ever modern wingsuit was developed by Patrick de Gayardon, which allowed him to glide through the air like a bird for about a minute and opened his parachute after he lost enough altitude, granting him the nickname of "bird man". A few years later after his tragic death during a skydiving accident,

in 1999 the first wingsuit company was established and was named “Birdman” in de Gayardon’s honor. In more recent years many companies have imitated his wingsuit design and made them widely available for the public [1].

Figure 1. Wingsuit inlets under the armpits and between the legs marked by red arrows.

Figure 2. A close-up of a reinforced wingsuit ram-air inlet.

1.2. Current wingsuit designs

A wingsuit is a personal flight device intimately connected to the body, designed to alter the body shape in order to maximize the user freefall time and glide ratio. [5] The basic principle of a wingsuit is to generate lift by adding surface area using an appropriate flexible fabric spread between each arm and the body, called the wings, and between the legs, called the tail. In order to do it efficiently it requires an airfoil profile which can be achieved by using the same double-skinned, cellular, ram air design used for modern skydiving parachutes and paragliders. The airfoil shape is maintained by ram-air pressure within the hollow airfoil sections of the wings and tail, which is delivered to the suit through some small inlets. These small inlets strategically positioned on the surface of the suit receive the ram-air and pressurize the airfoil shape of the suit, as shown in Figures 1 and 2. Wingsuits have no mechanical nor supportive structure or otherwise, the only rigid frame is the body of the flyer, thus all the aerodynamic forces are transferred directly the pilot’s body, offering humans the opportunity to experience flight in much the same way a bird does.

1.2.1. Structure and airfoil shape

Currently the arm wing and the leg wing designs of wingsuits are ram-air inflated through some inlets located on the surface of the suit and have an internal flexible fabric rib structure that is meant to allow them to get an airfoil shape in flight. This kind of structure is the same as the one used in common aircrafts, the only difference is the material; in aircrafts are made of metal while in ram-air parachutes, parafoils and wingsuits, are made of fabric. As shown in the following Figure 3, the structure of a wingsuit wing looks very similar to an aircraft wing without a spar. In the case of the wingsuit arm wing, the human arm serves as the spar and the leading edge support, and equivalently the human leg for the leg wing.

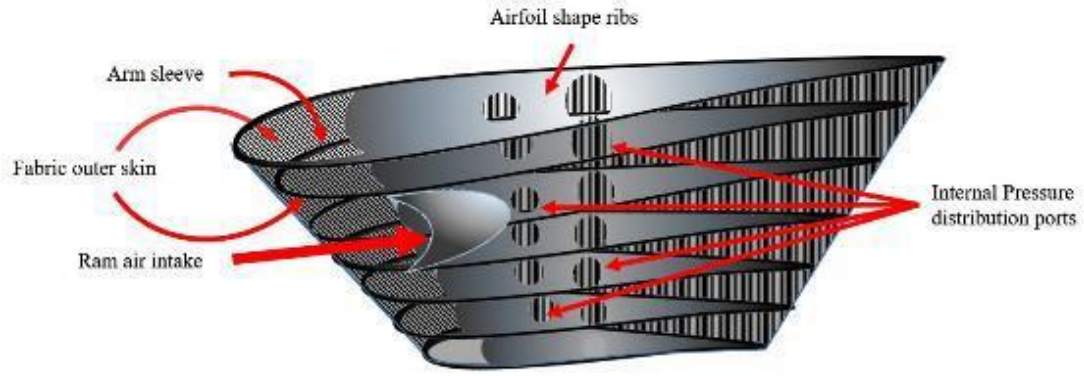

Figure 3. Diagram of ram-air inflated wingsuit wing structure.

Nowadays, there exists little information about the selection process of airfoils that can be used for the design of a wingsuit. The type of airfoil used for the wings is selected without much solid engineering or scientific basis. According to Uragallo (founder of Tonysuits, designer and flyer of wingsuit), evidence from some wingsuit manufacturers indicates that the airfoils used in wingsuit construction are generally chosen or altered to first fit the shape of the human body, and that this selection of airfoils is an inexact process on which many are selected by trial and error. This is mainly due to the fact that current wingsuit designs must be custom fit to the pilot's body, therefore the thickness, chord, and airfoil cross section of wingsuit wings are entirely variable.

Overall, wingsuit designs essentially encase the human body in a large ram-air inflated, fabric-clad wing that is able to provide an airfoil cross section. Even though, as mentioned before, there is not a systematic way of choosing the airfoil shape for a wingsuit design, it is

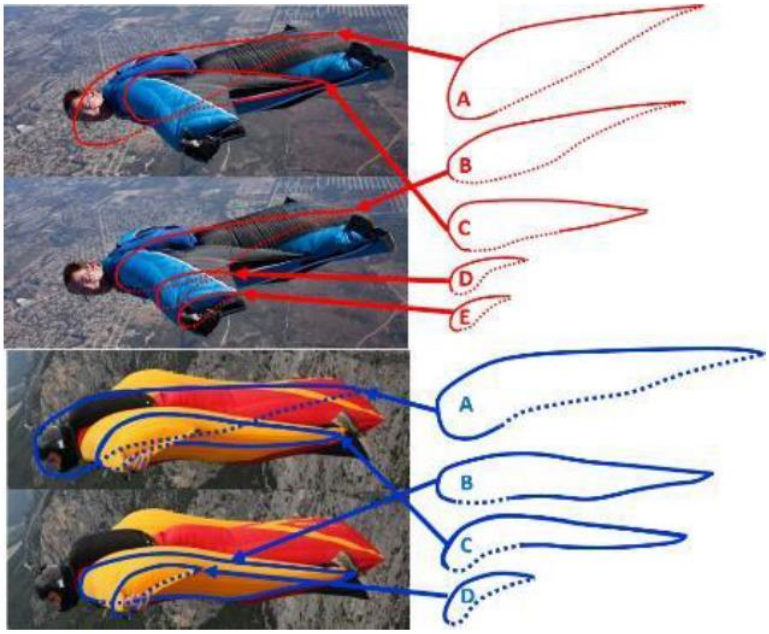

Figure 4. Technique used to estimate the airfoil shape of a wingsuit.

possible to estimate the airfoil cross section of a wingsuit by tracing the outline of the wing cross sections or airfoil shapes on a photograph of a wingsuit in steady flight. Sestak (2017) employed this technique, as shown in Figure 4, in order to estimate the chord, maximum thickness and camber of the airfoils; later on the average airfoil shape from the measured wingsuit, a design by TonySuits, was superimposed to the 50th percentile male body profile in a flight position, and after some analysis the NACA 4418 airfoil was selected as the average airfoil shape, Figure 5.

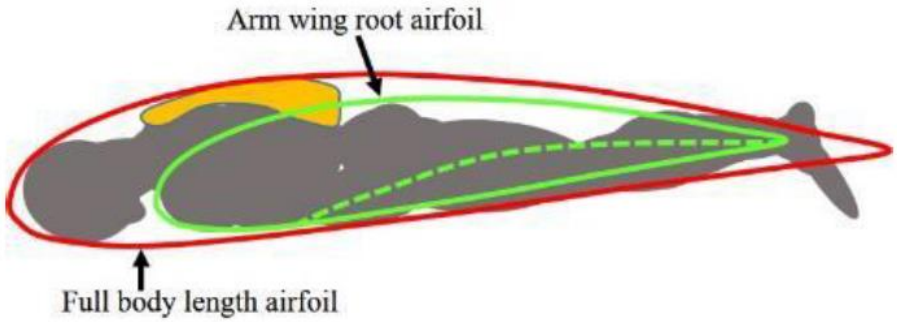

Figure 5. NACA 4418 airfoils superimposed on 50th percentile male body with parachute container, in flight position. Dotted line shows common lower cambered surface in wingsuit.

1.2.2. Wing configuration, planform and aspect ratio

The planform of an aircraft is the projected silhouette of the aircraft when seen from directly above. It shows the shape and size of the wings, and important parameters like wing shape, wing span, surface area, wing taper and wing chord. In order to generate a general planform of a wingsuit, a technique similar to the one used to get the airfoil can be used. This consist in tracing the outline on various pictures of wingsuits, both in flight and with people wearing them posing on the ground.

In a wingsuit planform, no matter the level of the wingsuit design, a delta or trapezoidal shape can be seen on the leg wing. An aft delta wing with a spanwise camber and leading edge anhedral is formed by the legs and the membrane between them, shown in Figure 6. Delta wings are generally low aspect ratio wings that taper to a point and generate high lift and high drag at high angles of attack. Anhedral has been shown to increase lift and reduce drag in highly swept delta wings with both spanwise chord and linear anhedral profiles (Traub, 2000). Even though a wingsuit has blunt leading edges and uneven surfaces, the wingsuit leg wing configuration is a configuration with the potential to generate significant lift (Luckring, 2002). The body of the pilot ahead of the leg wing have a significant aerodynamic effect on the leg wing, and a line down the body center from head to the trailing edge of the leg wing is the longest length on the wingsuit planform.

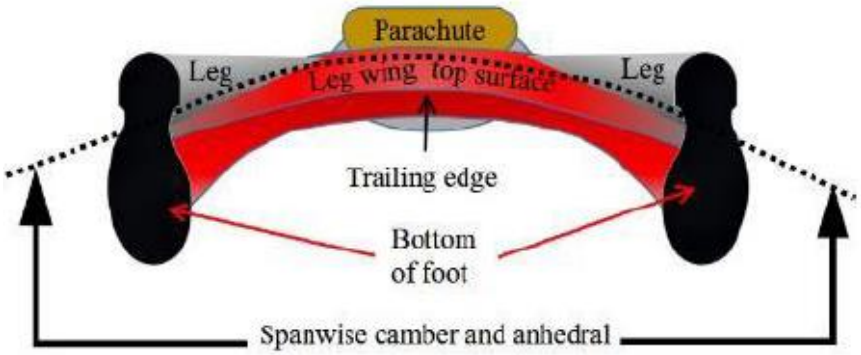

Figure 6. Diagram of wingsuit leg wing from behind, showing spanwise camber and anhedral.

From the planform drawing, several characteristics of the wingsuit can be determined, such as wing area S, chord c, span b, and aspect ratio (AR), which are also basic characteristics of a wing. The aspect ratio AR is a structural feature that has significant aerodynamics effects, and is defined as the wingspan b divided by the average chord $\bar{C}$. (Anderson, 2005).

$$AR = \frac{b}{\bar{C}} \quad (1)$$

If a wing is more irregular, such as tapered or other wings without a constant chord and the average chord is difficult to obtain, the AR can be defined as the square of the wingspan b divided by the wing area S. (Anderson, 2005).

$$AR = \frac{b^2}{S} \quad (2)$$

By looking at these equations is to say that wings with low AR are short, thick wings, and wings with high AR are long, thin wings. AR directly affect the lift and drag of a wing; a high aspect ratio generally gives higher lift and lower drag. Therefore, for the same wing surface area, a high aspect ratio wing is preferred.

1.2.3. Wingsuit dimensions and Reynold's number

Reynolds number is one of the most important factors used to describe or predict the characteristic of fluid flow, such as viscosity, shear stress, and compressibility, which are needed to find the pressure fields surrounding a wing, the high pressure and low pressure that creates lift, drag, and the wing vortex. It is a dimensionless value that expresses the ratio of inertial forces and viscous forces in a fluid like air (Kumar, Marshall, & De Remer, 2005).

In the case of wingsuits, Reynolds number determines the nature of the airflow over the wingsuit surface. For a high Reynolds number, inertial forces dominate in the fluid and the flow is more turbulent; for low Reynolds number viscous forces dominate and the flow is more smooth and laminar.

The formula of Reynolds number is as follows:

$$Re = \frac{VL}{v} = \frac{\rho VL}{\mu} \quad (3)$$

where V is the velocity, L is the characteristic length, ν the kinematic viscosity, ρ is the density of the fluid and μ the dynamic viscosity of the fluid. The chord of the airfoil is the characteristic length most often used for Reynolds number and aerodynamic lift.

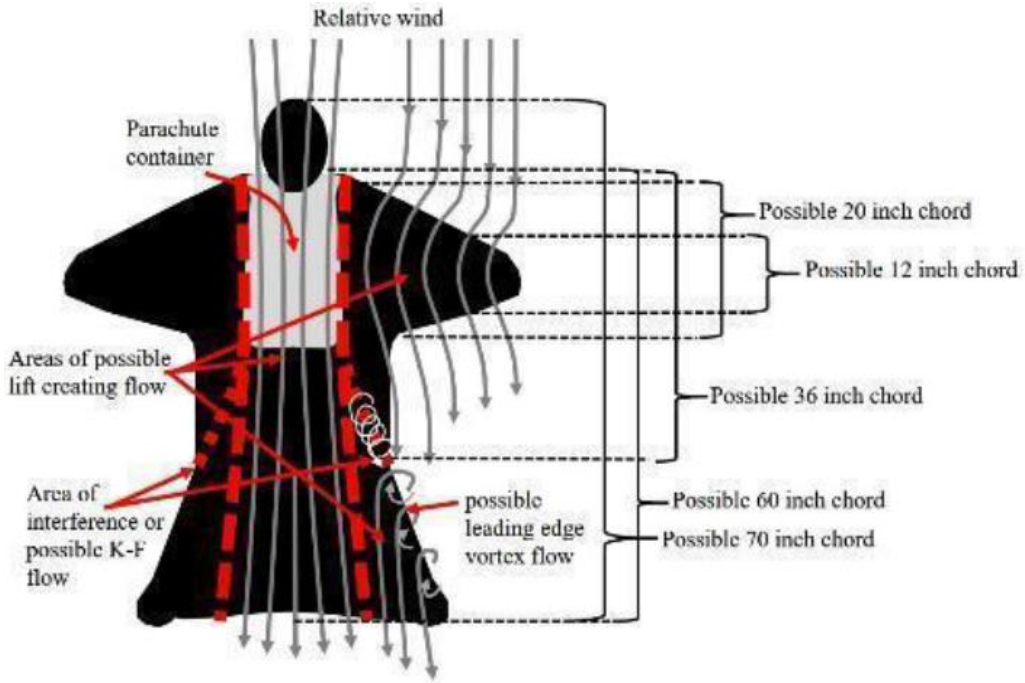

Figure 7. Planform of a wingsuit showing characteristic lengths for the calculation of Reynolds number.

According to Robson & D'Andrea (2010), wingsuit airspeeds range from 30 m/s to 90 m/s. Using the shortest characteristic length, 30.48 cm (12 in), and longest characteristic length 177.8 cm (70 in), as shown in Figure 7, with the lowest airspeed and highest airspeed, respectively, the range of Reynolds numbers applicable to wingsuits in flight can be calculated. For this, the kinematic viscosity of air at an altitude of 1524 m MSL is ν=1.65x10^{-5} m^2/s. Therefore, the range of Reynolds numbers for the full range of wingsuit flight is from 500,000 to 5.7x10^6 (Sestak, 2017). The range of Reynolds number must be taken into account for any meaningful analysis of wingsuit aerodynamics.

1.2.4. Beginner level wingsuit

The beginner level wingsuits are meant to train people new to the sport and safely give them experience to perform all the maneuvers necessary for wingsuit flight. Their design makes them more stable, therefore easier to fly, more comfortable and less restrictive than more

advanced wingsuits. Usually on the beginner wingsuit designs the arm wings and leg wing are completely separated, and all the parachute controls and risers are easily accessible to the pilot without having to unzip or release the wings. Beginner level wingsuits are essentially tandem winged aircraft (Kumar, Marshall, and De Remer, 2005) with the wings one behind the other on the same plane, when flying in the straight and level face down position.

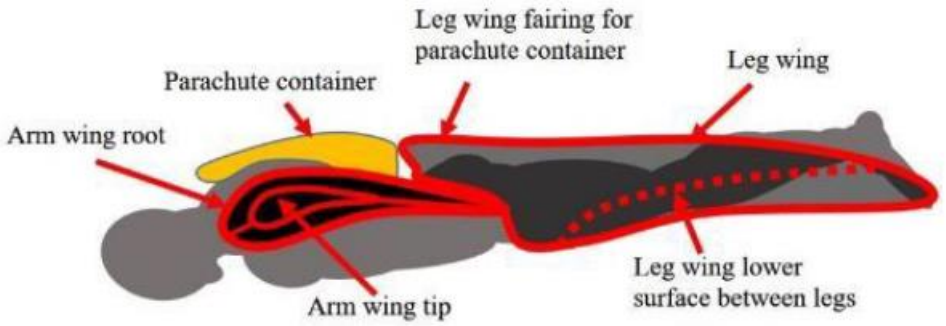

Figure 8. Profile diagram of tandem placement arm and leg wings on beginner level wingsuit.

Beginner level wingsuits have a trapezoidal arm wing with variable dihedral and anhedral controlled by the pilot's arms. The arm wing can also be swept aft with the consequence of creating slack in the material of the wing which makes it to billow upward and reduces the stability and rigidity of the airfoil. The forward arm wing is a two surface wing with a chordwise airfoil cross section. The leg wing is a truncated delta or triangular leg wing with an approximately 70° sweep. The relative position of arm and leg wings is shown in Figure 8. A normalized planform of beginner level wingsuits scaled for the 50th percentile American male (Panero & Zelnik, 1979) is shown in Figure 9. According to Sestak (2017), based on this scale, the aspect ratio for a beginner level wingsuit is approximately AR = 4.5 for the arm wing and AR = 1.1 for the leg wing.

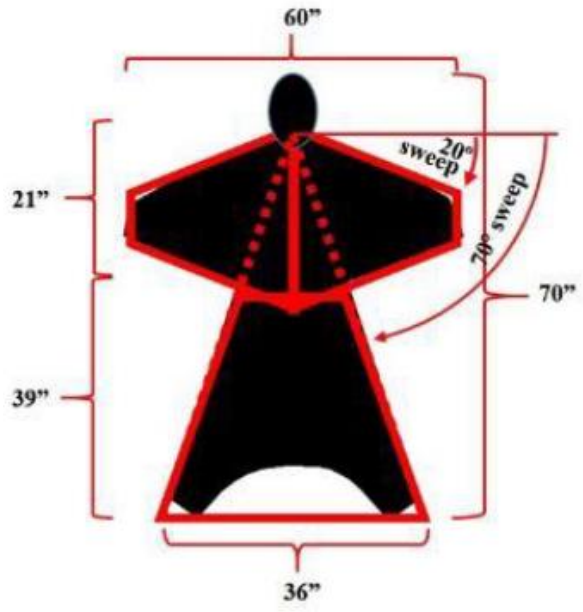

Figure 9. General planform of a beginner level wingsuit scaled for the 50th percentile American male.

In a wingsuit, the flight control is achieved through changing shape and position of the wings by coordinated movements of the pilot's body. A subtle body motion, such as turning the pilot's head left and right, pointing one toe while keeping the other foot in bent position, or changing the pitch of an extended hand, can be enough to initiate turns while in flight. To have a greater control on stability, lift, pitch, attitude, airspeed and rate of descent, the pilot can move the arms upwards in order to create greater dihedral.

1.2.5. Intermediate level wingsuits

Between beginner and advanced level wingsuit designs there exist many different size, shape, and wing size and position. The intermediate level wingsuits specialize for different purposes, some are specialized for speed, others for acrobatics and some are specially designed for BASE jumping. Because of this, intermediate wingsuit planforms have a wider range of planforms, but have the same construction techniques of ram air inflated designs as the beginner level wingsuits.

The arm wings of intermediate level wingsuits have larger total wing area, and the leg wings have a wider leg separation; the trailing edges of the arm wings are lengthened down the outside edges of the leg wing. Also the seep, taper and length of the wings are different. Some common intermediate wingsuit planforms are shown in Figure 10. Therefore, these

modifications increase the AR, compared to the beginner wingsuits, as the surface area increases with no change in span, which are in the range of 2.5 or lower. [6]

So the main differences between beginner and intermediate level wingsuits are the root chord and tip chord of the arm wings and the and the length of any extension of the arm wing down the leg of the pilot. The tip chord of the arm wing of intermediate level wingsuits is often increased by the addition of a rigid rod in the wing tip. The pilot holds this rod and can deflect it up or down to help control the wing aerodynamics. Usually the trailing edges of the arm wings are attached to the leading edge of the leg wing. This creates an area of potential interference with the smooth, aerodynamic flow up and around the leading edges of the leg delta wing, caused by the juxtaposition of the trailing edge of the arm wing and the leading edge of the leg wing.

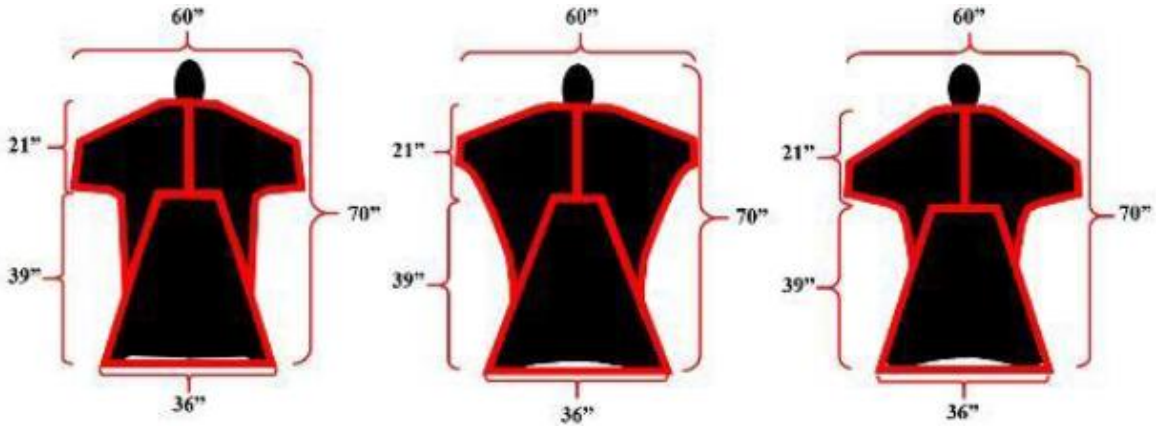

Figure 10. Common intermediate wingsuit planform scaled to the 50th percent American male.

1.2.6. Advanced level wingsuits

The advanced level wingsuits are the largest, have the highest performance and are the least stable of all. These wingsuits have very large wings that are joined to the leg wings continuously along the leg wing leading edge to the feet of the pilot, making them one large, uninterrupted surface. Also, the leg wing is extended beyond the pilot's feet. According to wingsuit pilots, a minimum of 150 wingsuit jumps is recommended before try to fly advanced level wingsuits.

Advanced level wingsuits have ram air inflated wings and airfoil shapes just like the beginner and intermediate level wingsuits. The attempt to create as much area surface as possible in current wingsuits has driven all expert level wingsuits to a low AR rectangular

planform. (Birdman International Ltd., 2013). They have longer extensions of the arm wings with a stiffening rod in the wingtip chord, to increase the wingspan, the wingtip is often canted outward, and to increase the surface area, the leg wing is often extended behind the pilot's feet. In Figure 11, three common expert wingsuit planform designs.

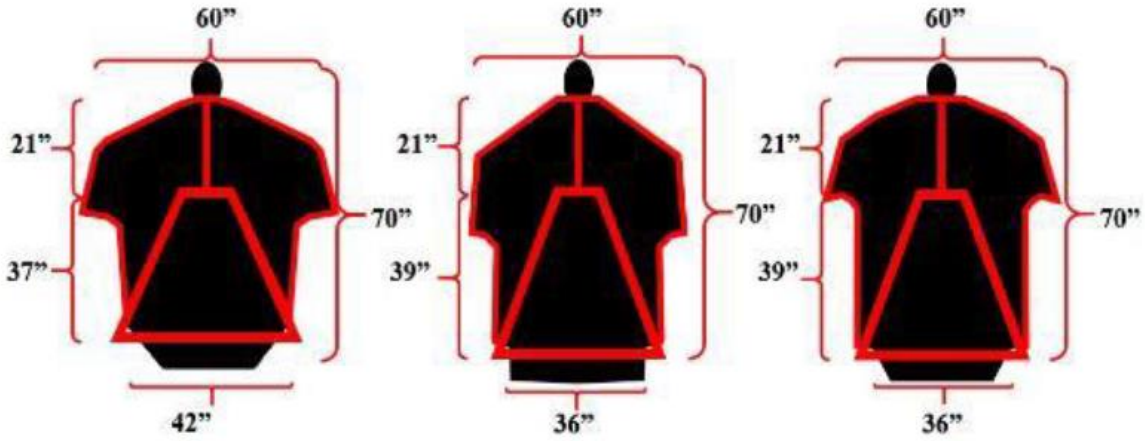

Figure 11. Common expert wingsuit planform scaled to the 50th percent American male.

According to Sestak, 2016, the surface area of the leftmost suit in Figure 11 is approximately 23 ft^2, and its $AR = \frac{5.3^2}{23} = 1.2$, while the center wingsuit in Figure 11 has an aspect ratio of $AR = \frac{4.67^2}{22} = 0.99$. In current configurations, these large, single surface wingsuits are limited by the dimensions of the human body and generally assume the shape of a very low aspect ratio rectangle.

Because the trailing edge of the extension of the arm wing is connected all the way down to the ankle of the pilot, the flow over the leading edge of the leg wing has been completely eliminated. This configuration makes the aerodynamics more complicated, because the arm wing and the leg wing both have airfoil shapes, but they are connected, as shown in Figure 12, making the wingsuit one surface with no continuous airfoil shape. The leg wing can no longer act as a separate wing; there is no airflow from below the leg wing over the leading edge of the leg wing.

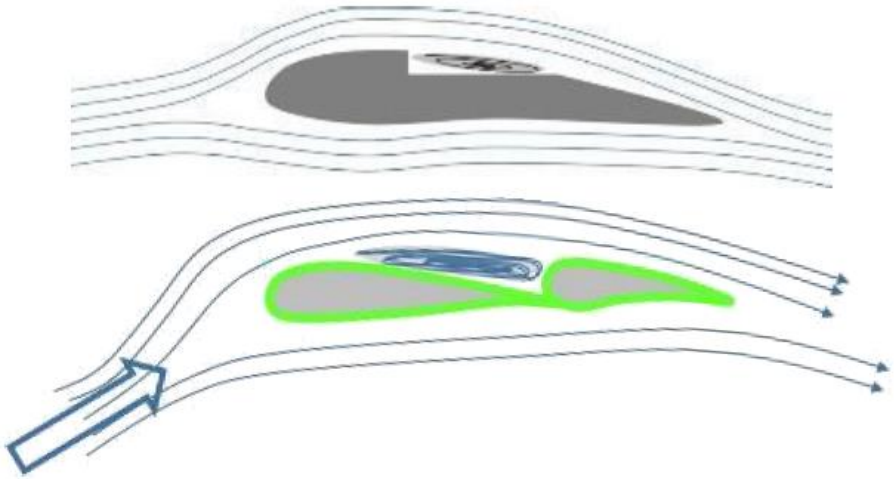

Figure 12. Upper illustration: simple diagram of an upper surface notched K-F airfoil with trapped vortex and freestream airflow. Lower illustration, possible K-F flow in wingsuit arm wing - leg wing interference area.

1.3. Motivation

Even though wingsuit design has gradually evolved from the first flights by Patrick de Gayardon in the 1990s, and flight performance has improved significantly (Abrams, 2003), wingsuit flying is still considered a new sport and it is now deemed one of the world's most dangerous sports. Although during the last two decades it has slowly gained some popularity, it has been a slow process and to date the wingsuit community is still small. As a result, it lacks of formal testing resources and not a lot of scientific research has been done regarding this sport.

Most of the researches that have been done mainly focus in increasing the glide ratio by increasing the area of the wingsuit, which seems to be already at its limit. Much of the progress in wingsuits to date has been by trial and error and, despite claims of aerodynamic research and several groups investigating wingsuit performance in wind tunnels, the aerodynamics of wingsuits remains largely undetermined (Higgins, 2015).

Therefore, we have decided to conduct a thorough study of some already existent wingsuit designs and make on them some modifications and compare them in order to determine which is the most relevant part of the suit for creating lift, whether is the wings or the tail. By doing so, we want our study to be of great help for future wingsuit related studies, as a way to contribute for achieving a better performance and maneuverability of wingsuits, increase the safety of wingsuit flight and decrease the rate of fatal accidents within this wonderful sport.

2. Experimental overview

During this experiment we chose two already existent wingsuit designs by Squirrel Wingsuits [12], the GÜS (Figure 13), a wingsuit for beginners, and the AURA 3 (Figure 14), a wingsuit for advanced pilots, to which we made a few modifications. We used the software CATIA to draw the 3D models; in total we 3D printed ten scaled models, five scale models of each wingsuit design. One model has no changes, is simply a scale or the original design, while for the other four some modifications were made on the design and areas of the wings and tails. All ten models were tested in a water tunnel located in the Aeronautics and Astronautics department of National Cheng Kung University, where we were able to watch the behavior of the flow. Based on the pictures obtained during the experiment of the flow around each model we determined which of these models have better flow behavior, taking in consideration the flow separation and vortex creation.

Figure 13. GUS design wingsuit

Figure 14. AURA design wingsuit

2.1. Significance of study

There are several groups currently working on wingsuit performance improvements as the general mindset of the sport transitions from one of trial and error to the application of technology and scientific principles (Bisharat, 2015). We found out that there is little scientific studies and documentation regarding aerodynamics, control and design of wingsuits.

However, information about this sport is gradually increasing and shows its potential beyond thrill seeking and captures the interest of a variety of academic experts. An examination of the factors involved in current wingsuit design are crucial for deciding the direction of future development. Current wingsuit designs can seldom fly more than 2 or three minutes when launched from normal skydiving altitudes. We believe that increasing the glide ratio of the wingsuit will enable the wingsuit to be used for non-sport implementation such as developing for military applications.

Wing design parameters are constrained, in the case of wingsuits, by human body dimensions and strength issues. The human frame and muscular strength are the equivalent of spars, wing ribs, and frames in a conventional aircraft: this imposes more restrictions on the wingsuit design since the strength of the average human cannot be readily changed. (Engin & Kaleps, 1980; Robson & D'Andrea, 2010).

Current designs use certain body positions that require significantly less strength to hold than other positions. Allowing the arms wings to bend upward with the lift force reduces pressure but results in an increased rate of descent and in a lower glide ratio. Ideal wing designs would create the center of lift pressure as close inboard to the body center line as possible while still maintaining a desirable gliding ratio and not requiring excessive human strength. Moving the center of pressure of the wing inboard would reduce the strength requirements of human arms and legs in wingsuit flight.

2.2. Purpose

The purpose of this research study was to determine through experimental testing in a water tunnel the effect that different wing designs have on the aerodynamic efficiency of the wingsuit using flow visualization techniques. To understand by analyzing the visualization, the reason why currently used wingsuit has a certain shape and to determine if there is any possibility of perfecting the design by altering the shape of the wings.

In addition, to show by inspection what part of the wingsuit may produce higher lift on the model, whether is the arm wings or the leg wings, therefore having a higher gliding ratio.

2.3. Aims and objectives

Aims

1. To determine the part of a wingsuit that induces more lift, whether is the arm wings or the leg wing.
2. To determine how different wingsuit designs, affect the aerodynamic performance and stability of wingsuit flight.
3. To understand the reason of different wingsuit designs for different performance level; i.e. to understand why beginner and advanced level wingsuit models have different designs.

Objectives

1. To visualize and understand the flow structure on the surroundings of the wingsuit using ink flow method. This includes laminar to turbulent flow separations and vortices generated at the proximities of the wingsuit for understanding the phenomena that takes place at the wingsuit's surface.
2. To visualize the flow on the surface of the wingsuit using the red dot method. This includes detecting the reattachment line and vortices generated at the surface.
3. To obtain instantaneous velocity measurement and related properties of the flow using Particle Image Velocimetry (PIV) method. This includes Velocity magnitude vectors and vorticity of the flow, with respect of the vectoral translations of the particles.

3. Methodology

3.1. Research approach

Water tunnel study was selected as the appropriate method for wingsuit flow visualization. The ability to record phenomena at Reynolds numbers similar to that at which wingsuits normally operate is important because the factors involved in working with three-dimensional wingsuit models would be difficult to scale.

Control of water flow speed, AOA, and different arm and leg designs were other primary considerations of the water tunnel study.

The selection of the range of AOA from 5 to 25 degrees reflects the average angles of wingsuits during steady flight. Negative AOA, which would represent inverted flight, was not considered in this study. While wingsuits are currently flown inverted, they are not flown

inverted for maximum performance; in fact, performance is significantly degraded while flying inverted. For the wingsuit design selection, we have choses the beginner and advanced wingsuits. The beginner wingsuit is designed for easily and control and parachute deployment by the pilot. The advanced wingsuit is for experienced pilots and for flying at higher speeds. Then we changed each model's arm wings and leg wings, in order to visualize and analyze the flow.

3.2. Experiment designs and procedures

The methodology after that we have chosen for this experiment is the following

1. Selection of appropriate beginner and advanced design wingsuit models.
2. Using computer aided design software Catia, model the wingsuit models.
3. Having the water tunnel specifications, calculate the aspect ratio (AR) and the blockage ratio of the model's blockage ratio of the models.
4. Create or obtain a support that fits on the water tunnel for holding the models.
5. Modify each wingsuit model. Change the arm structure and the leg structure of both beginner and advanced models. Each wingsuit is then modeled as a new design. This results in five models for beginner wingsuit and five models for the advanced wingsuit. Draw a special base on each model that fits into the support.
6. 3D-print all the wingsuit models at the appropriate size depending of the water tunnel's cross-sectional area.
7. Water tunnel testing begins with the red ink flow method and the red dot method, in order to get results describing the flow surrounding the model and at the model's surface respectively.
8. Choose the two most aerodynamically efficient models, one beginner and one advanced.
9. Particle Image Velocimetry (PIV) begins. Set up ion lasers and high-speed camera. Get particle simulation data including animation for visualization of velocity profile of each wingsuit.

3.2.1. Models design

The 3D model designs were drawn using the CATIA software. In the case of the water tunnel test, we first scaled down the wingsuit designs to a length from hand to hand of 160 mm, a parameter that we chose for convenience, and after this we calculated the blockage ratio to make sure it has a value of less than 10%.

We modified the area and design of the wings without changing the tail, one model with bigger area and another model with smaller area, and vice versa, when modified the tail, the wings remained the same. In order to know the difference among the models of each design used for testing, each model was labeled with a specific name depending on the area that was modified, whether was the area of the wings or of the tail, as shown in Table 1.

Name	Description
Original	Has no changes, is just a scale of the original design
Arms 1	Area of wings is smaller, area of tail remains the same
Arms 2	Area of wings is bigger, area of tail remains the same
Legs 1	Area of tail is smaller, area of wings remain the same
Legs 2	Area of tail is bigger, area of wings remain the same

Table 1. Label and description of each model

The thickness of our 3D models is the same for all, 3 mm. In addition, each model has a base especially designed to fit the support built for the water tunnel tests. After having all the designs ready, we proceeded to 3D print them using 1.75 mm PLA white wire. Afterwards, a layer of white spray paint was applied to each of them, and then, using different sizes of sand paper, P100 and then P800, their surface was made smoother for better results of the water flow over the surface.

Figure 15. 3D printed models with label. Top row, advanced level (AURA) design. Bottom row, beginner level (GUS) design. The “GUS original” model of the beginner level design is missing in this picture.

In Figure 15 we show all the models labeled just after they were 3D printed. For an easier understanding, we further explain the labels used for each model. We refer to each model first by its real design, whether is GUS (beginner level) or AURA (advanced level) design, and then by its redesign label which are shown in Table 1. So on figure 15, top row from left to right the models are as follows: Aura original, Aura arms 1, Aura arms 2, Aura legs 1, and Aura legs 2; bottom row from left to right are: GUS arms 1, GUS arms 2, GUS legs 1, and GUS legs 2 (in this picture the GUS original model is missing).

As can be seen in figure 16, horizontal lines with 1 centimeter of separation were drawn along the surface of all the models as a guide to achieve a better visualization of the flow behavior.

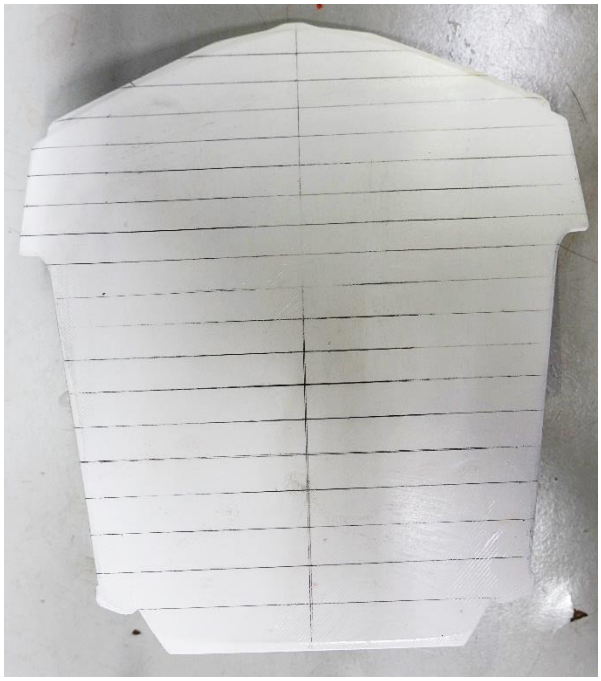

Figure 16. Guidelines over models with 1 cm separation.

The GUS design has two leading edges, one at the arm wings and the second one at the leg wings, and in consequence it also has two trailing edges, while the AURA design only has one leading edge and one trailing edge. The different edges for both models are shown in figure 17 at an angle of attack of 5°.

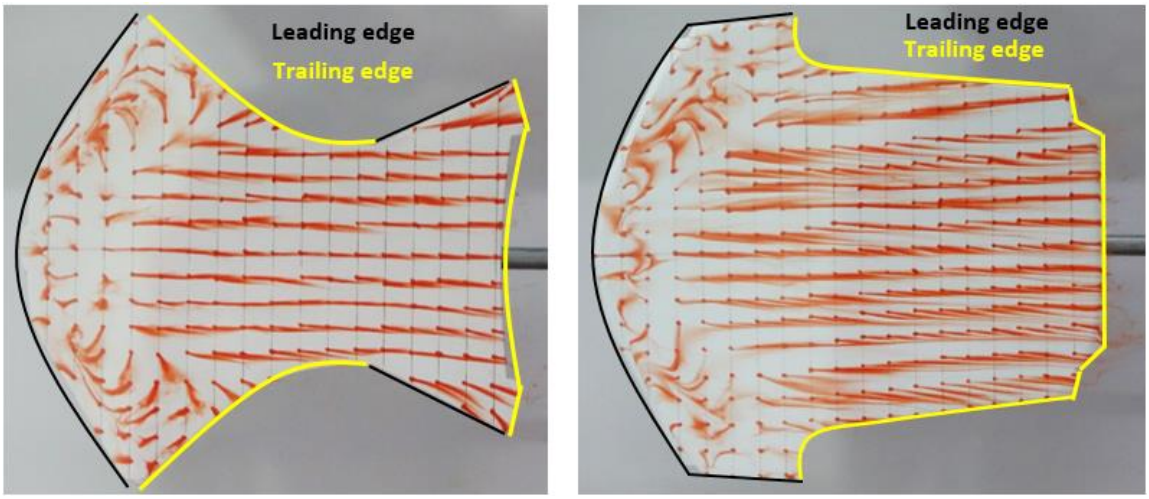

(a) GUS Original (b) AURA Original

Figure 17. Red dot method, leading and trailing edges of GUS and AURA Original designs at α = 5°.

3.2.2. Parameters

Here we explain how some of the most important parameters needed for the experiments we conducted were found and calculated; these include aspect ratio (AR), blockage ratio, and Reynolds number (Re).

3.2.2.1. Aspect ratio

As explained before, the aspect ratio is an important characteristic of the wing with important aerodynamic effects. Sestak (2017), shows that the aspect ratio of the arm wing for a beginner level wingsuit scaled for the for the 5'10" tall, 50th percentile American male (NASA, 1995), is $AR = 4.5$. For intermediate level wingsuits, on which the surface area of the arm wing increases with no change in span, the AR is reduced to about 2.5 or lower. While for expert level wingsuits, because they are single surface wingsuits, the AR is even less, depending on the design, the AR is usually around 1.

For the case of this experiment, first we found the total surface area of each model and their respective wingspan. Afterwards, Equation (2) was used to calculate the aspect ratio of our models. Below we show a table for each model design, beginner and advanced, including these parameters.

Model	Beginner level (GUS)			Advanced level (AURA)		
	Wingspan (cm)	Surface area (cm^2)	AR	Wingspan (cm)	Surface area (cm^2)	AR
Original	16.476	180	1.51	17.365	250.22	1.21
Arms 1	16.476	170	1.60	17.365	239.68	1.26
Arms 2	16.476	190	1.43	17.365	259.25	1.16
Leg 1	16.476	180	1.51	17.365	245.09	1.23
Leg 2	16.476	190	1.43	17.365	255.85	1.18

Table 2. Aspect ratio of each model

3.2.2.2. Blockage ratio

In order to have good results, it is recommended that blockage, the ratio of frontal cross section of the test wing to the area of the test section, be less than 0.1 (Barlow, Rae, & Pope, 1999), this is, less than 10%.

$$Blockage\ ratio = \frac{frontal\ cross\ section\ of\ test\ wing}{area\ of\ test\ section} \times 100 \qquad (4)$$

Therefore, the dimension of our models was chosen according to the blockage limit. First we assumed the length of hand to hand for both wingsuit designs to be 160 mm, which gives a wingspan of 164.7 mm for the beginner design, and 173.6 mm for the advanced design. Then we obtained the projected cross section area of each model at the maximum angle of attack (AOA) used for this experiment, this is $\alpha = 25°$. Because the water tunnel used has a test section area of $3600\ cm^2$, the blockage ratio equation becomes

$$Blockage\ ratio = \frac{A_{wingsuit,25°}}{3600\ cm^2} \times 100 \qquad (5)$$

Therefore, to make sure that our scaled models were suitable for testing, using equation (5) the blockage ratio for each model was calculated. This is shown in Table 3, along with the frontal cross section area of each model at $\alpha = 25°$.

Model	Beginner level (GUS)		Advanced level (AURA)	
	$A_{wingsuit,25°}$ (cm2)	Blockage ratio	$A_{wingsuit,25°}$ (cm2)	Blockage ratio
Original	82.3	2.29%	153.7	4.27%
Arms 1	79.4	2.21%	150.3	4.18%
Arms 2	87.8	2.44%	155.5	4.32%
Legs 1	80.5	2.24%	151.8	4.22%
Legs 2	83.9	2.33%	156.1	4.34%

Table 3. Cross section area at $\alpha = 25°$ and blockage ratio of each model

As it can be seen, the maximum blockage of the current setup is less than 3%, therefore, the dimensions that we assumed are proper for our experiment.

3.2.2.3. Reynolds number

As mentioned before, the Reynolds number is a very important parameter used to describe the degree of laminar or turbulent flow. Any system that operates at same Reynolds number will have the same flow characteristics even if the fluid, speed and characteristic lengths are different. In the case of the water tunnel tests the Reynolds number for each model were calculated using Equation (3) as follows:

$$Re = \frac{997\left(\frac{kg}{m^3}\right) \times 0.089\left(\frac{m}{s}\right) \times MAC\ (m)}{0.8937 \times 10^{-3}(\frac{kg}{m} \cdot s)} \tag{6}$$

where $V = 0.089\ m/s$ is the water flow velocity, $\rho = 997\ kg/m^3$ is the density of water, $\mu = 0.8937 \times 10^{-3}\ kg/m \cdot s$ is the dynamic viscosity of water and L is the MAC (Mean Aerodynamic Chord) of each model. Because the wingsuit models have irregular shapes, the MAC of each model was obtained by drawing nine evenly separated lines on the model with the help of the CATIA software and calculating their average chord length, as shown in the following Figure 18.

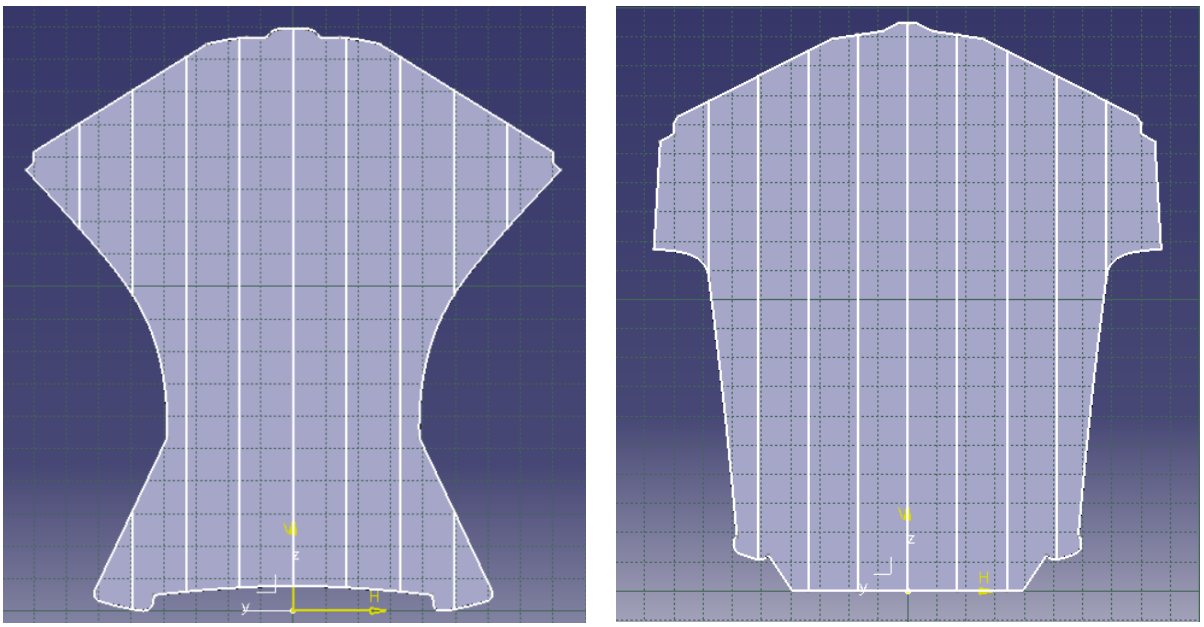

Figure 18. Method used to find the average chord length of models using CATIA. GUS (left) and AURA

Substituting the results of MAC for the scaled models of GUS and AURA 3 designs into equation (4) we were able to obtain the Reynolds number of each model. The values of MAC and their corresponding Reynolds number are shown in the following Table 4.

Model	GUS		AURA 3	
	MAC (m)	Re	MAC (m)	Re
Original	0.12141	12100	0.15561	15500
Arms 1	0.11669	11600	0.15304	15200
Arms 2	0.12964	12900	0.16455	16300
Legs 1	0.11855	11800	0.15224	15100
Legs 2	0.12403	12300	0.15844	15700

Table 4. MAC and Reynolds number of each model

These results were compared with the Reynolds number of full size wingsuits, calculated using the average airspeed of a wingsuit, 45 m/s, and the longest characteristic length of a full size wingsuit, 1.77 m. In this case, the values of density and dynamic viscosity of air at 1500 m above sea level were obtained by interpolating values from the U.S. Standard Atmospheric Air Properties table, which yield $\rho = 1.06\ kg/m^3$ and $\mu = 1.742 \times 10^{-5}\ kg/m \cdot s$. Putting these values into Equation (3) gives

$$Re = \frac{1.06\left(\frac{kg}{m^3}\right) \times 45\ \left(\frac{m}{s}\right) \times 1.77\ m}{1.742 \times 10^{-5}(\frac{kg}{m} \cdot s)} = 4.8 \times 10^6 \qquad (7)$$

This result is within the range of Reynolds number that Sestak (2017) found for the full range of wingsuit flight. Therefore, we can see that there is a big difference between the Reynolds number of our model and the Reynolds number of a real size wingsuit. According to the study by Chen H. et al. (2013) on delta wing performance, although the Re difference forbids a direct quantitative comparison between a real size wingsuit experiment and our

water tunnel flow experiment, it is reasonable to assume that the flow pattern in both cases will be fairly similar.

3.3. Experimental setup and materials

The water tunnel tests were conducted in the water tunnel located at the Department of Aeronautics and Astronautics Engineering in National Cheng Kung University, Tainan, Taiwan. This water tunnel has a test section of $60\ cm \times 60\ cm$, and is shown in Figure 19. In order to do the tests, a special base was needed to mount the models into the water tunnel.

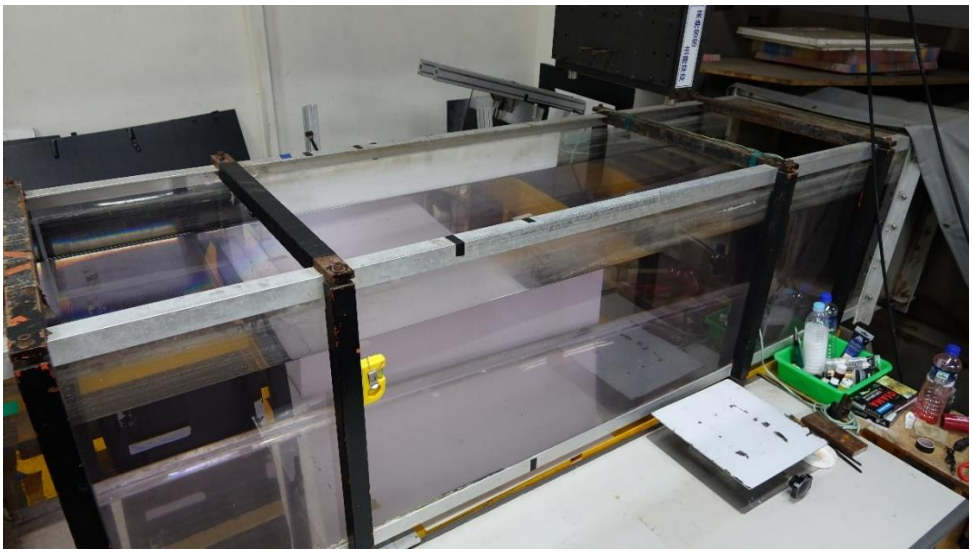

Figure 19. Water tunnel test section located in the Department of Aeronautics and Astronautics at National Cheng Kung University.

The base used for this experiment was already built by some master students that were conducting some tests in the water tunnel, and we borrowed it from them. This structure is made of aluminum; it consists of a flat piece of 60 cm length and 10 cm wide as support, that perfectly fit on the upper opened surface of the test section, and perpendicular to it another less wide and shorter piece is connected, which tip only reaches half of the water tunnel. A movable arrangement of a long thin tube of 9 mm diameter and a fixed protractor is set at the tip of this piece. The models are mounted to the long tube, and the protractor is used to measure the desired angle of attack. This base structure and the protractor are shown in Figure 20 and Figure 21, respectively.

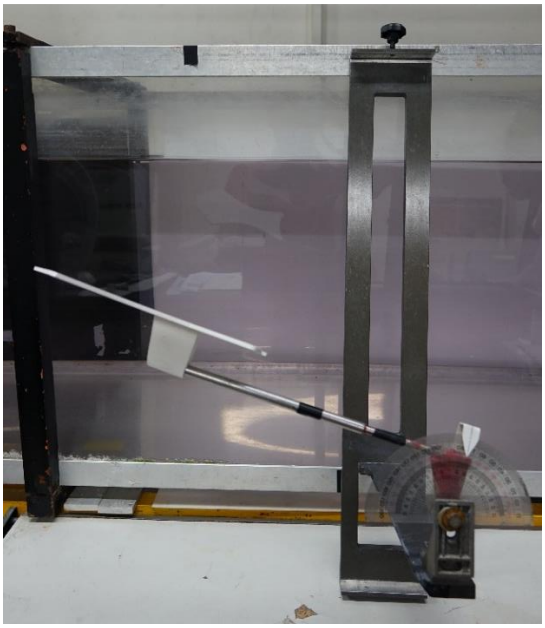

Figure 20. Base structure used to support the models for the water tunnel tests.

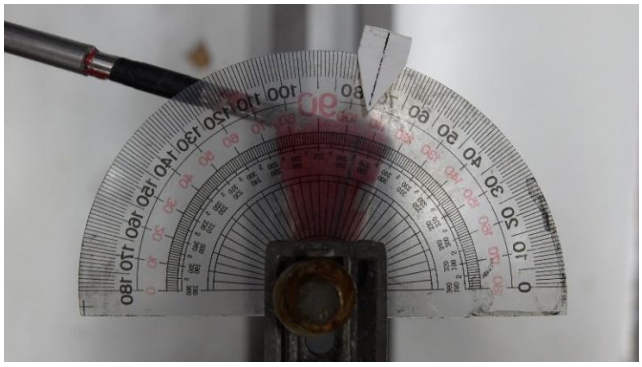

Figure 21. Protractor mounted on the support at an angle of attack of 15°.

The models, as mentioned before, were 3D printed, using 1.75 mm PLA white wire. A layer of white spray paint was applied to them, then sandpaper was used to make their surface smoother. We started with a P100 waterproof sandpaper, followed by a P800. For the ink flow test, food paint was used, and for the red dot test, water based paint and a fine brush was used, in both cases, color red was chosen for convenience of better visualization. Below is a table with all the materials and costs used for the water tunnel test, and a picture of some of these materials is shown in Figure 22.

Material	Quantity	Cost (NTD)	Total (NTD)
1.75 mm PLA white wire	1	360	360
P100 sandpaper	4	3	12
P800 sandpaper	4	3	12
Food paint (Red)	2	40	80
Acrylic paint (Red)	1	25	25
Paint brush (Size 0)	1	20	20
Spray paint (White)	2	65	130
Spray paint (Black)	1	65	65
			704

Table 5. Materials used and costs

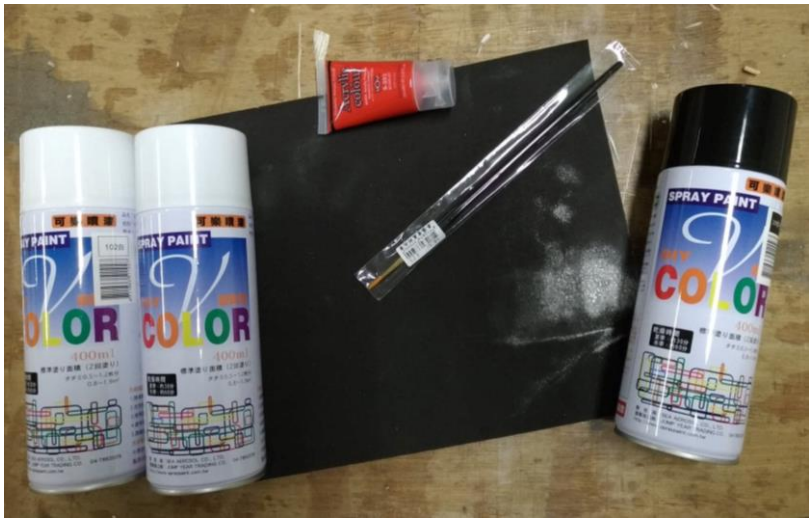

Figure 22. Materials used for the preparation of models for the water tunnel tests.

3.4. Water tunnel test

The water tunnel tests consist of two different tests, one using ink flow method and one using red dot method. With these methods we can view the flow around the models and the flow on their surface, therefore we are able to analyze different characteristics of the flow.

Water tunnel testing was completed using angles of attack from 5° to 25° in increments of 10 °, this means angles of 5°, 15° and 25°. This range correspond to the common angle of attack at which wingsuit pilots fly directly into the freestream. The wingsuit models were tested at water tunnel speed of 8.9 cm/s, calculated using the following formula:

$$U = 0.71 \times f + 0.39 \ \ (cm/s) \qquad (8)$$

Where f is the frequency from the frequency converter of the water tunnel used. This frequency was set as $f = 12\ Hz$.

A high resolution, fast speed Nikon camera borrowed from the Aeronautics and Astronautics department was used to take pictures and videos during the test. The settings of the camera for taking pictures was set to take a burst of five pictures with an interval of 0.3 seconds, while for the video it was set to 60 fps.

3.4.1. Ink flow method

For this test method we used the base structure previously mentioned that perfectly sits on top of the water tunnel, and to this we attached each model. We started testing the beginner level models using two different arrangements of ink flow simultaneously. One consisted of two thin hose with thin syringes on the tips attached to a bottle, and the other of one thin hose with an L shaped tube on its tip, attached to another bottle. Red food paint was dissolved with water and then poured into the bottles. Each hose had a device used to control the ink flow.

The two syringes were attached on the rear side of the model pointing against the water flow with its tips at the outer part of the arm wings just past the leading edge, while the L shaped tube was pointing towards the flow stream direction a few centimeters in front of the center line of the models. This creates three streamlines of ink, two at the outer part of the model and one at the center, with this we hoped to see the flow behavior over the arm wings and at the center of the model. In the Figure 23, this arrangement can be seen in action during a test made for the "original" model at $\alpha = 15°$.

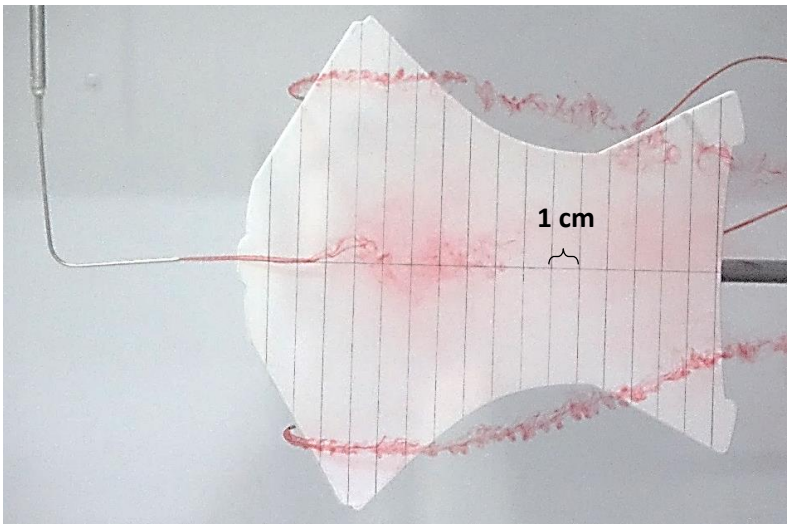

Figure 23. Arrangement used for the ink flow test. In the picture the "original GUS" model at an AOA of

3.4.2. Red dot method

The red dot method test consisted on drawing dots on the surface of the models along the guidelines, as shown in figure 24, in order to visualize the behavior of the flow over the surface. The paint used was a red color acrylic paint, and a size 0 paint brush was used to paint the

dots, which were located about 1 cm apart from each other. For this case, the same base structure was used to mount the models into the water tunnel.

The tests were conducted at angles of attack of 5°, 15° and 25°, with the free stream speed (water speed) previously mentioned. For the GUS design all the models were tested, while for the AURA design only Arms 1, Arms 2 and Original models were tested. With this test, the flow behavior on the surface was seen and some of the most relevant characteristics are analyzed along the following sections.

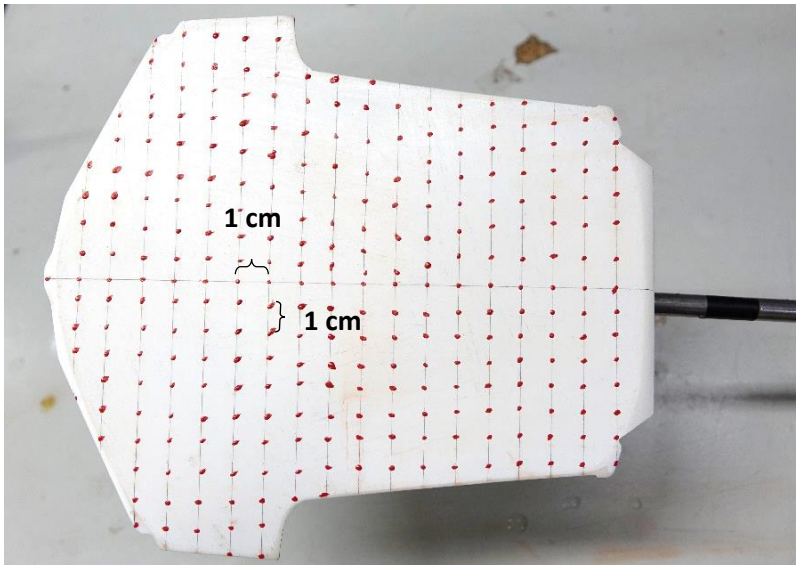

Figure 24. Models configuration of Red dot method test. In the picture “original Aura” design model.

3.4.3. PIV test

PIV, stands for Particle Image Velocimetry, is an experimental tool commonly used in fluid dynamics and aerodynamics. It is used to obtain instantaneous velocity measurements and related properties in fluids. The basic principle involves taking pictures at high frames per second of the motion of microscopic particles, illuminated in a plane of the flow with a laser beam, that follow the fluid flow. Image processing methods are then used to determine the particle motion, and hence the speed and direction of the flow (the velocity field), from the pictures.

In order to analyze the data obtained, the frames are split into large number of windows. This makes possible to calculate a displacement vector for each window with the

help of signal processing and autocorrelation techniques, which is then converted to a velocity using the time between frames and the physical size of each pixel on the camera.

The PIV tests were conducted for two models, the GUS Arms 2 and the Aura Arms 2, which were selected after analyzing the flow behavior obtained from the ink flow method and the red dot method tests. They were conducted at an angle of attack $\alpha = 15°$, which was considered to be the most relevant during previous test and the average AOA during a wingsuit flight. The model was held by a special support borrowed from the water tunnel lab, and an L shaped ruler was used to measure the size of the particles and pixels by putting it in the water tunnel besides the support and model, as shown in figure 25.

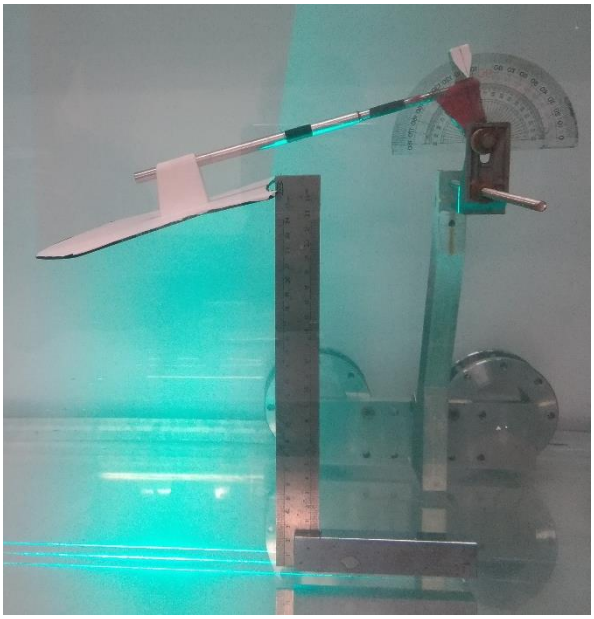

Figure 25. Model support and scale method of PIV test.

The laser arrangement at the water tunnel in the department of Aeronautics and Astronautics in NCKU consisted of a high power Coherent Innova ion laser system located under the water tunnel, which beam was aimed upwards (shown in figure 26). A Redlake N-4 high speed camera was used to obtain the images, with a configuration of 200 frames per second for a total of 6.3 seconds, a delay time of 5 ms, an exposure of 2 ms, and ROI (region of interest) of 1016 X 720. The whole setup while testing is shown in figure 27.

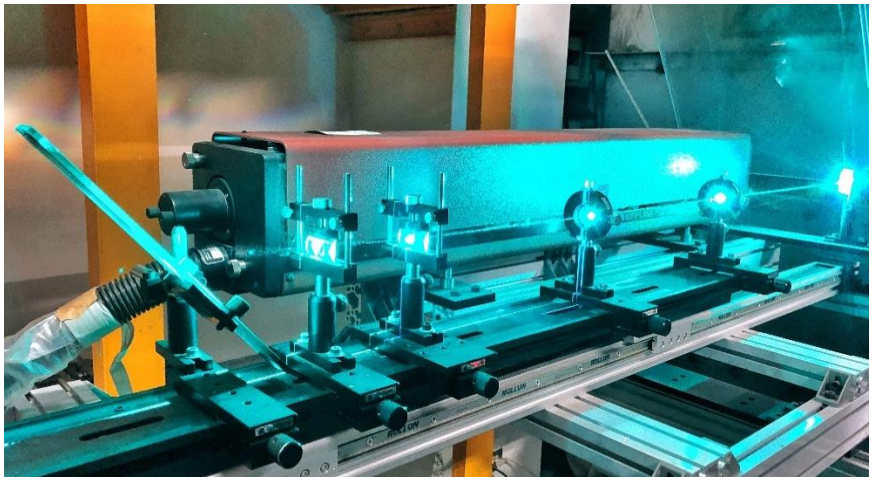

Figure 26. Ion laser system used during the PIV tests.

For the data analysis the PIV View 2C software was used to obtain the velocity field of the flow and then Tecplot 360 was used to visualize the data. Within the PIV View software an interrogation size needed to be calculated in order to get accurate results, for this the following formula was used:

$$\frac{1}{4}\ interrogation\ size\ \geq\ M \times V_0 \times \Delta t$$

where,

$$M = magnification\ factor = \frac{pixels}{scale\ distance\ (mm)}$$

$$V_0 = flow\ velocity\ (\frac{m}{s})$$

$$\Delta t = delay\ time\ between\ each\ frame\ (s)$$

Careful attention need to be paid on the units which should give pixels for the minimum interrogation size.

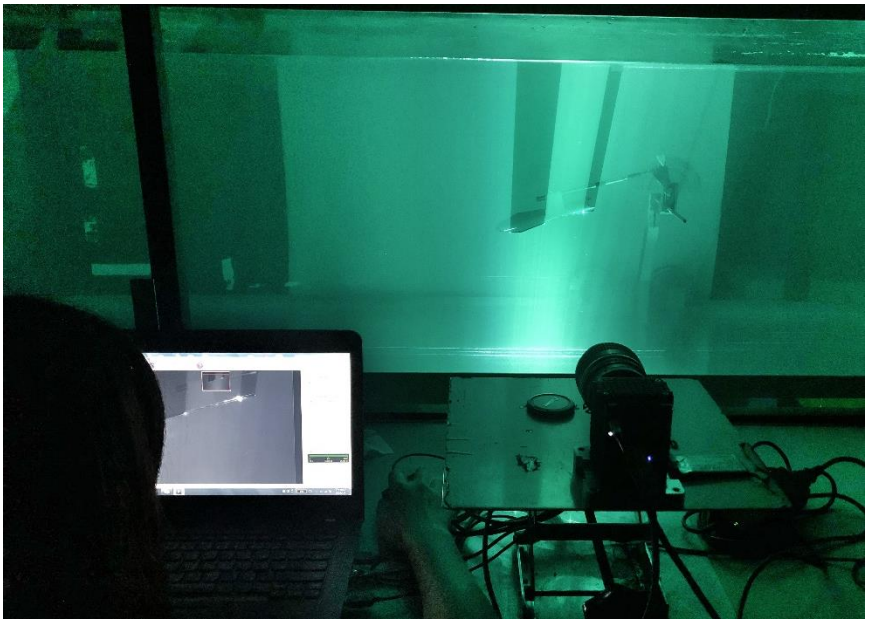

Figure 27. PIV experiment setup while in use.

4. Results and discussion

Some pictures obtained during the water tunnel experiments from the ink flow method for GUS design and the red dot method for GUS and AURA designs, are arranged and shown below, in figure 28, 29 and 30 respectively. These pictures show all the different design models tested at the three different angles of attack selected for this experiment.

For the ink flow test, the flow visualization showed the flow behavior over the models, and in this part only the most dominant features will be emphasized. A comparison of beginner level wingsuit models at different angles of attack is made, this is shown in Figure 28, which shows typical flow visualization images obtained at angle of attack, $\alpha = 5°$, $\alpha = 15°$, and $\alpha = 25°$ for a range of Reynolds number $11600 < Re < 12900$.

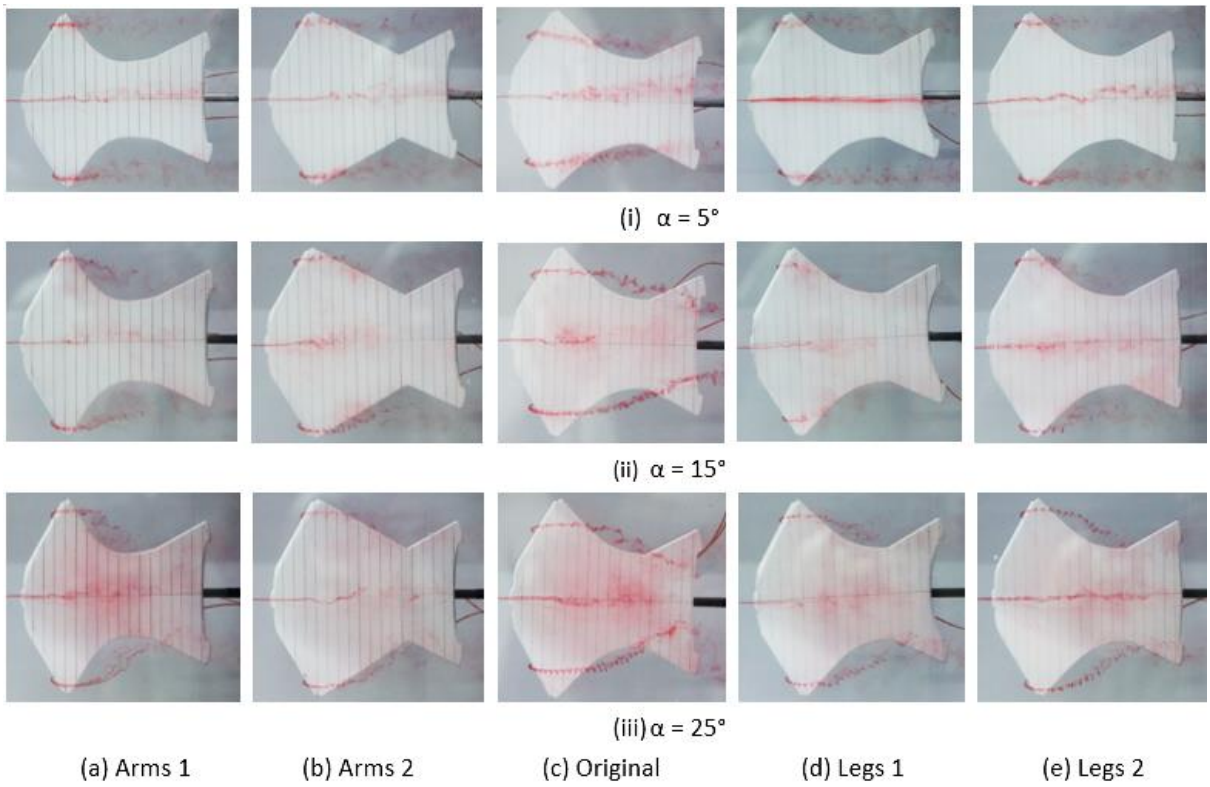

Figure 28. Ink flow method, beginner level (GUS) design models at different AOA.

For the case of the ink flow method, all the GUS design models were tested and none of the Aura design models were tested. This is because the flow visualization using the ink flow method was mainly the flow separation point and the curvature of the outer streaks, which did not tell us much about the behavior of the lift over the surface of the wingsuit models, and considering that the models of the advanced level wingsuit are also flat and have just small changes on their design, just like those of the beginner level, we decided to not do the ink flow method test with the advanced level models, and assumed the results will be similar.

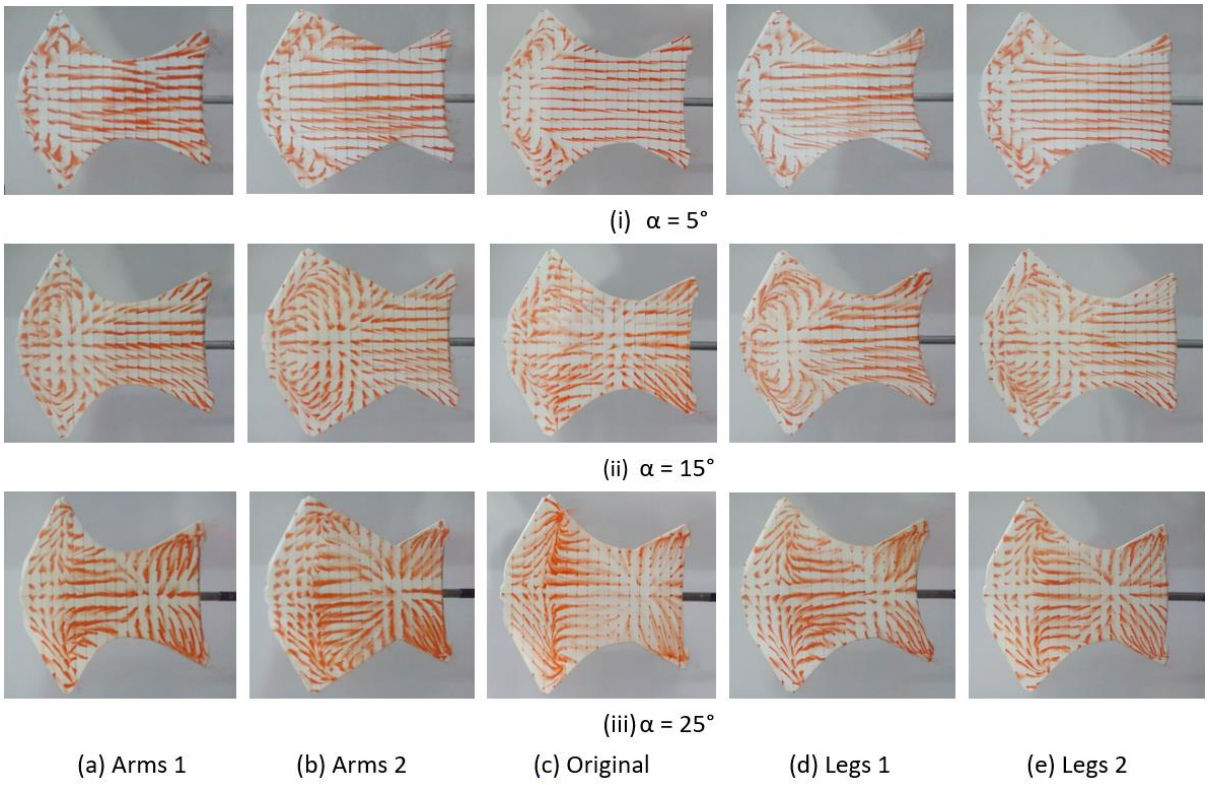

Figure 29. Red dot method, beginner level (GUS) design models at different AOA.

According to the results obtained from the GUS designs during the red dot method test, the flow characteristics are mostly present on the area of the arm wings, therefore, we conclude that the lifting forces are mostly generated near the leading edge and are more significant on the arms. Because of this, for the advanced (AURA) design the “Legs” models were not tested, and all the following results are more focused on the original, arms 1, and arms 2 of both GUS and Aura design models.

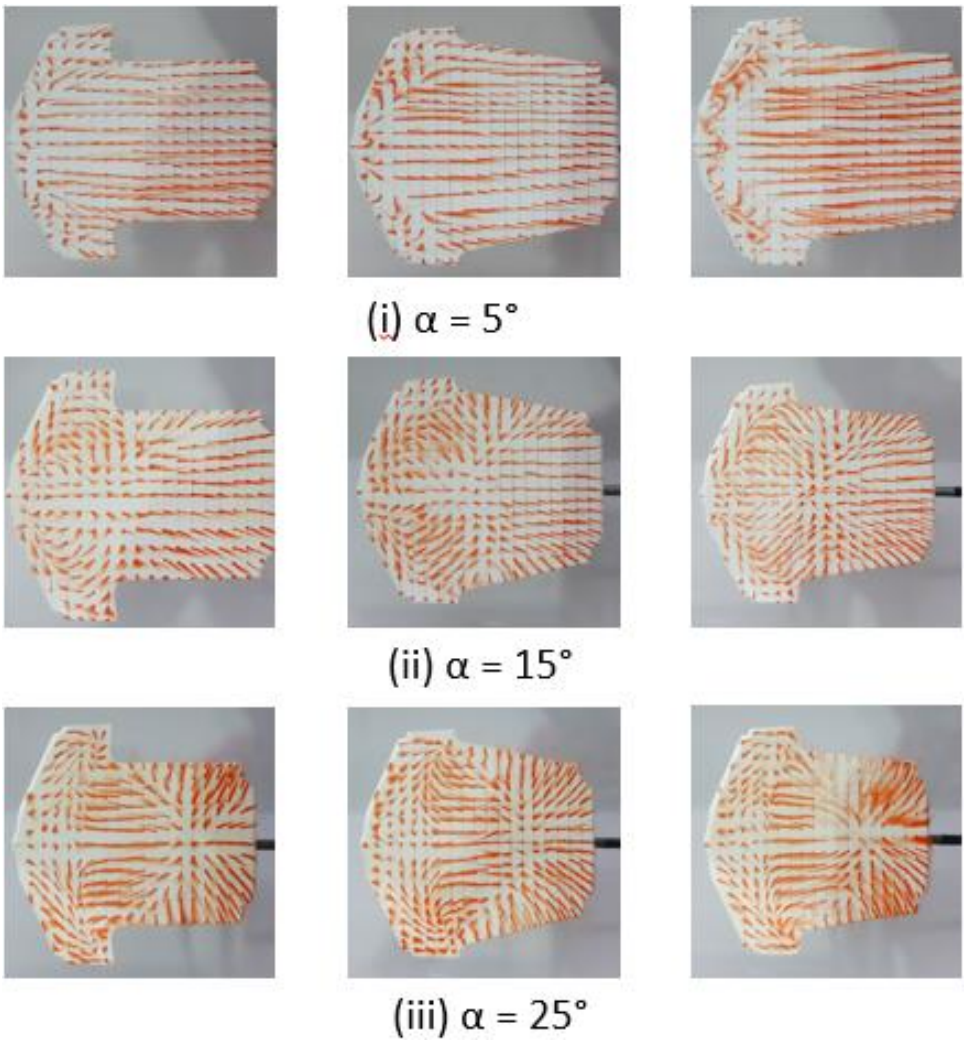

(a) Arms 1 (b) Arms 2 (c) Original

Figure 30. Red dot method, advanced level (AURA) design models at different AOA.

At first glance, the flow phenomena of the AURA models are similar at each angle of attack regardless of their arm structure. They all behave in similar manner, shifting the flow separation line as proportionally as the angle of attack is increased, and generating good looking vortex geometries at the wings. The reason why there are not much flow geometric variations in the models is partly because they all share a similar rectangular shape, and the modification of wing structures are small compared to the area of the model.

4.1. Original model

Here, the GUS and Aura original models are analyzed to describe, from the flow visualization, the flow behavior and the flow characteristics over the surface. In this case, the results are

shown for the ink flow method and red dot method, with an angle of attack of α = 15°. Symmetry about the centerline is assumed for all the following results.

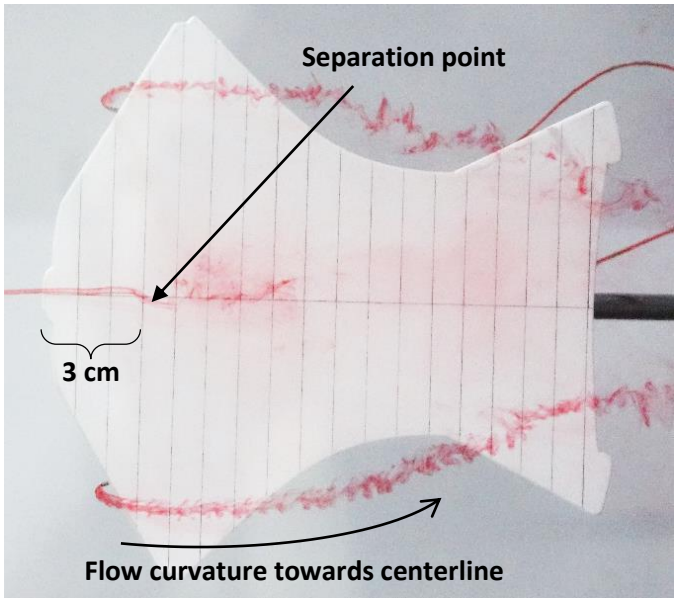

Figure 31. Flow characteristics over GUS original model at α = 15°.

For the case of GUS original at AOA of 15°, the middle streak clearly has a flow separation point located at 3 cm away from the leading edge, at which the flow becomes turbulent and the dye simply expands as it flows downstream. The outer streaks have spirals formed at the leading edge that flows downstream and towards the centerline.

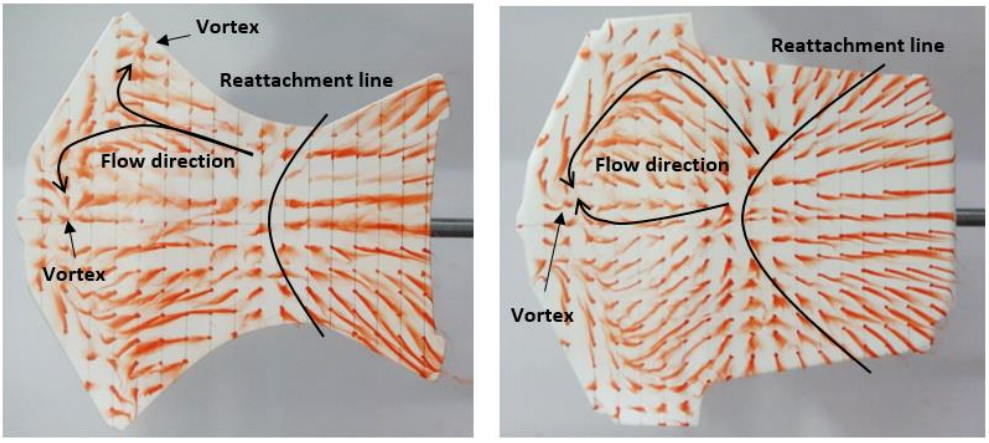

(a) GUS Original (b) AURA Original

Figure 32. Red dot method, flow characteristics of GUS and AURA Original designs at α = 15°.

GUS original model at 15° has several changes in flow direction and a total of 4 vortices located at approximately 1 cm and 7 cm from the centerline to both sides. In contrast, for AURA original model at 15° the reversed flow direction is inwards, towards the centerline, where two vortices are created about 1 cm away from the centerline.

4.2. Arm design effect

4.2.1. Ink flow method

GUS models

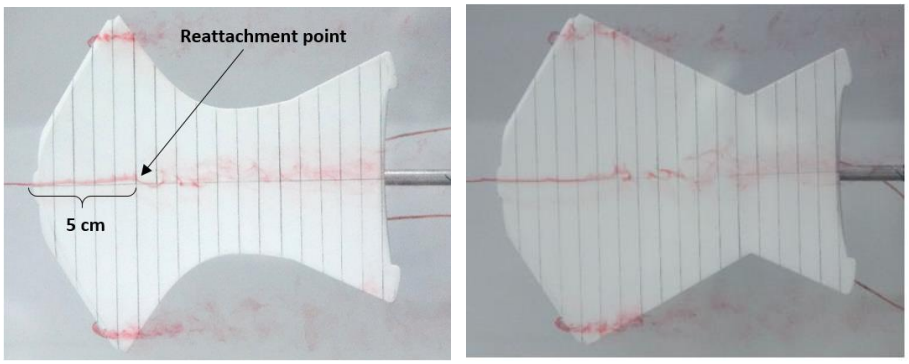

α = 5°

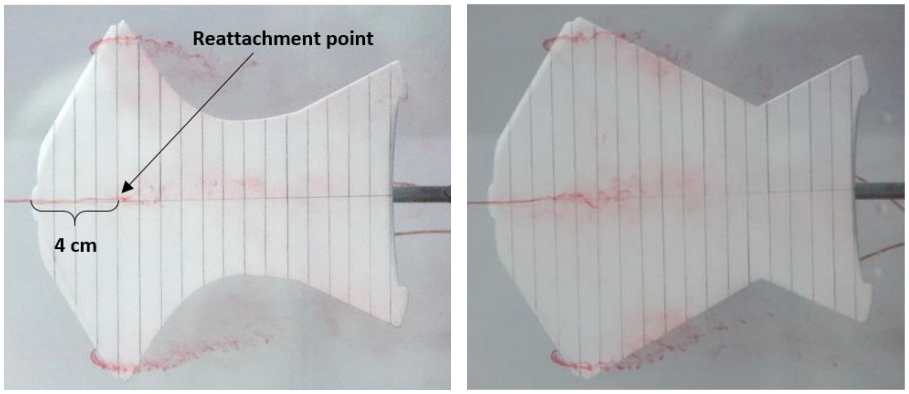

α =15°

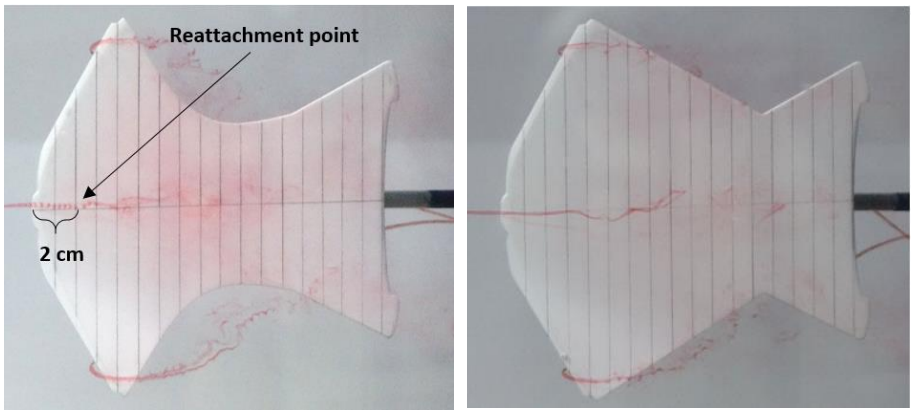

α =25°

Figure 33. GUS arms 1 (left) and arms 2 (right) during ink flow method test at different AOA.

For the GUS design, with different Arms design, shown in figure 33, the outer streaks flow behavior varies, while the middle streak remains almost the same. Regarding the curvature of the outer streaks, the GUS arms 1 model show a sharper bend and the GUS arms 2 model show a less pronounced curve.

For Arms 1 model, the separation point at α = 5° is about 5 cm from the leading edge; at α = 15° is about 4 cm from the leading edge; at α = 25° is about 2 cm from the leading edge.

4.2.2. Red dot method

GUS models

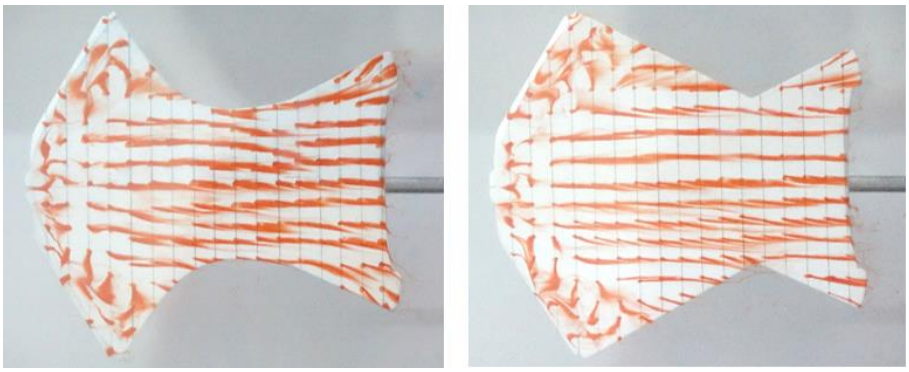

α = 5°

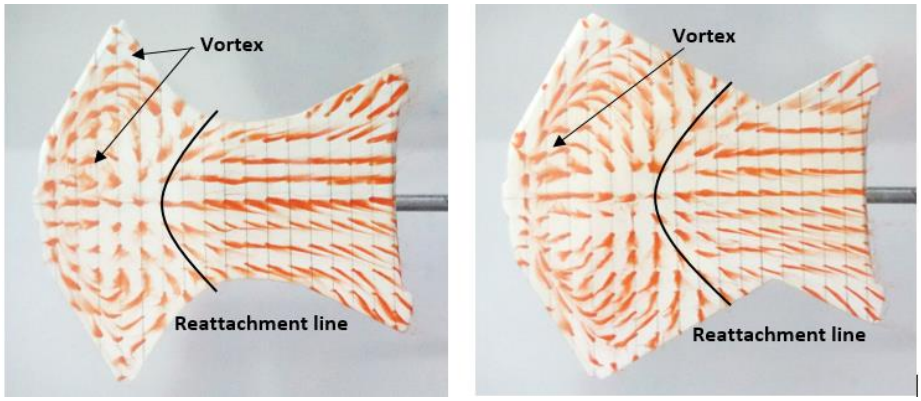

α = 15°

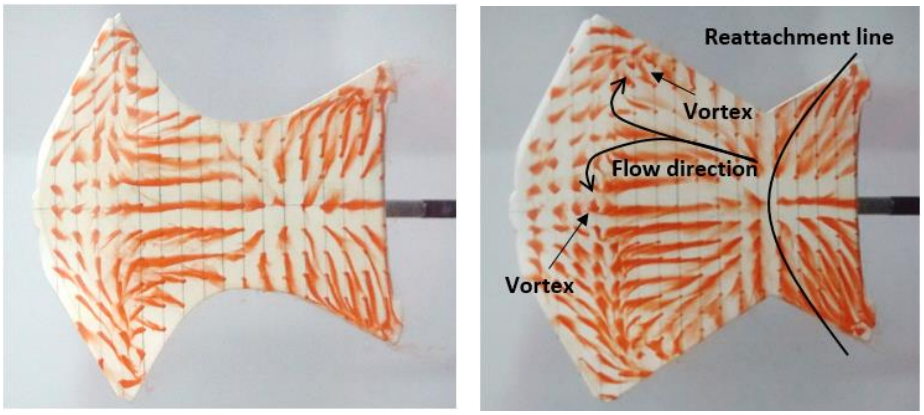

α = 25°

Figure 34. GUS arms 1 (left) and arms 2 (right) during red dot method test at different AOA.

For red dot method test of different GUS arms design models, shown in figure 34, the flow behavior changes significantly with different design and also with different angle of attack, being more notorious over the arm wings. Differently, the flow behavior over the leg wing remains the same with different design models (Arms 1 and Arms 2) and with different AOA.

As can be seen at α = 15° the vertex of the reattachment line for the Arms 1 model is located 1 cm earlier than that of the Arms 2. This is about 6 cm away from the leading edge for the Arms 1 and about 7 cm away from the leading edge for the Arms 2.

The Arms 1 design has a total of four vortices on the arm wings, two at each side of the centerline, one at 1.5 cm from the leading edge and 1 cm away from the centerline, and the other 4.5 cm away from the leading edge along the centerline and 6.5 cm away from the centerline. The “arms 2” design has just two vortices on the arm wings, one at each side of the centerline, located 1.5 cm away from the leading edge and 1 cm apart from the centerline.

AURA models

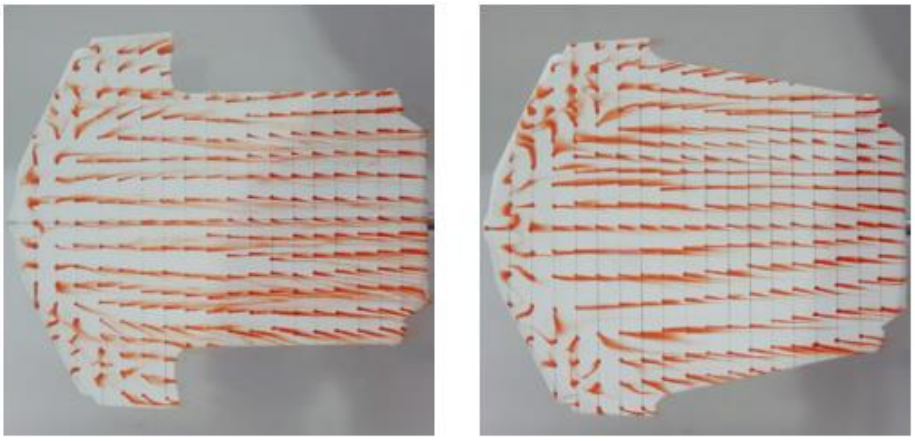

α = 5°

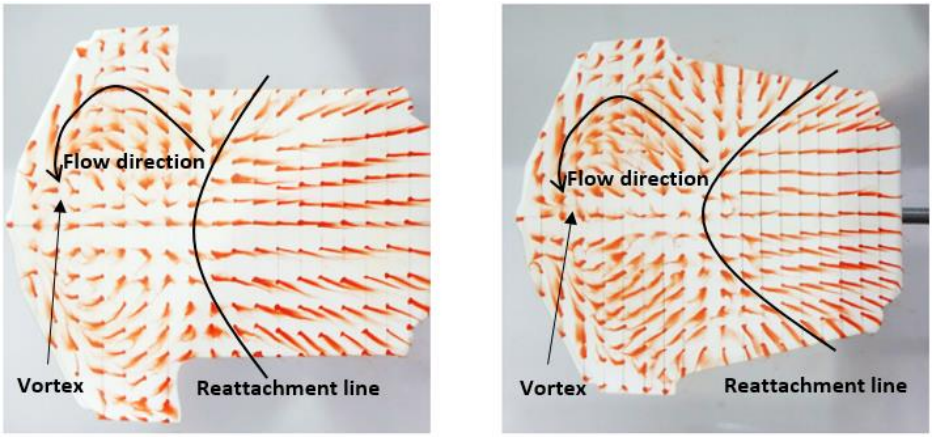

α = 15°

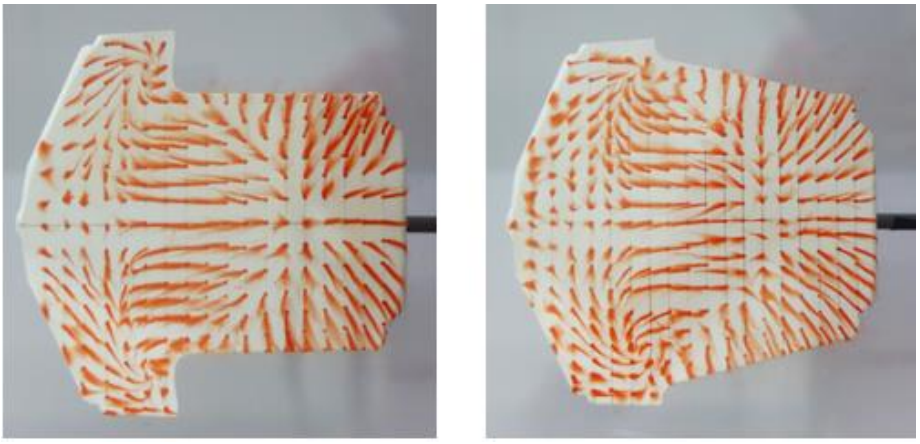

α = 25°

Figure 35. AURA arms 1 (left) and arms 2 (right) models during red dot method test at different AOA.

For the same angle of attack (α = 15°), the reattachment line of both Aura arms 1 and Aura arms 2 (shown in figure 35) models is located at a distance of about 7.5 cm from the leading

edge. However, due to their difference in design, they have different surface flow visualization before the separation line.

The Arms 1 design has two vortices on the arm wings, because of symmetry along the centerline, they are both located at 2.5cm from the leading edge and 2.5 cm away from the centerline. On the other hand, the Arms 2 design also has two vortices, at the same distance away from the centerline but 3.5 cm away from the leading edge. This happens because Arms 2 design has greater area than Arms 1. Because of this difference in design, arms 2 model has more distance for the vortex to prorogate throughout its area. For both models however, the flow after the centerline is equally laminar and without any disturbances or apparent phenomena.

4.3. Leg design effect

4.3.1. Ink flow method

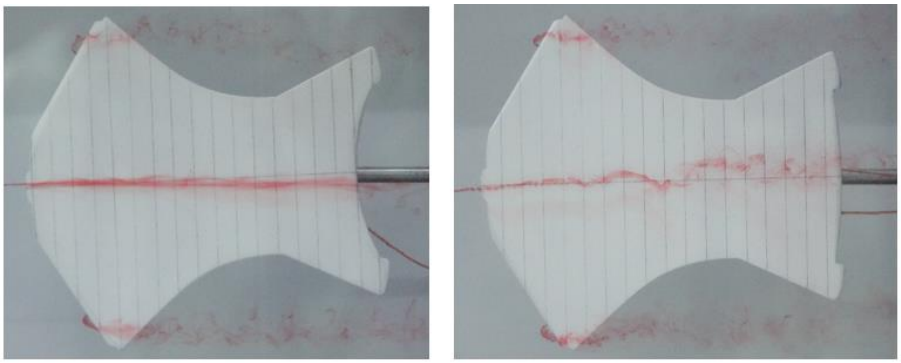

α = 15°

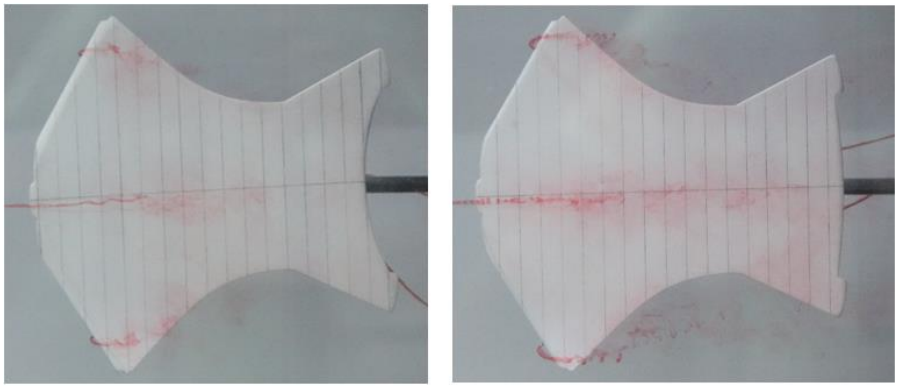

α =20°

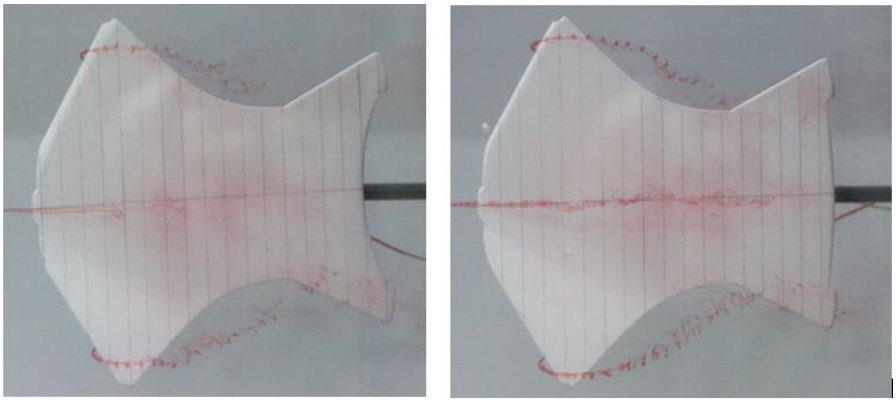

α =25°

Figure 36. GUS legs 1 (left) and legs 2 (right) during ink flow method test at different AOA.

For the case of GUS Legs 1 and GUS Legs 2 models (shown in figure 36), the dye streaks originating from almost the same outer locations have practically the same flow path all the way to the trailing edge, while for the middle streak is a similar case. All of these designs show no difference of flow behavior over the arm wings at and just a small difference of flow direction, starting 2 cm before the trailing edge, over the leg wings. Therefore, the flow behavior remains the same everywhere except near the trailing edge.

4.3.2. Red dot method

GUS models

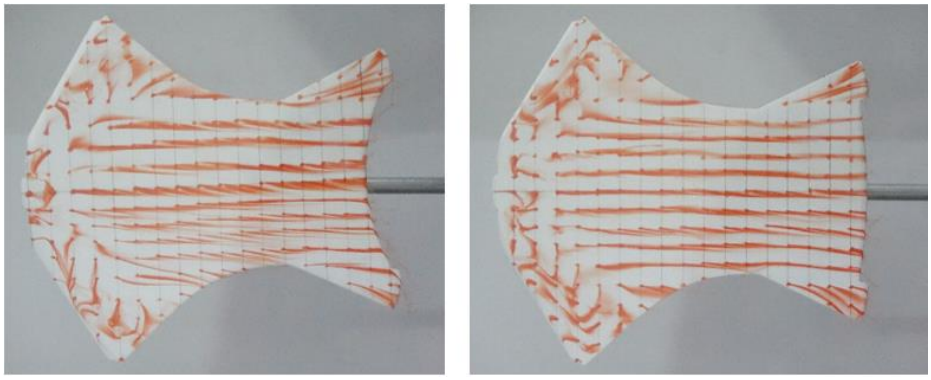

α = 5°

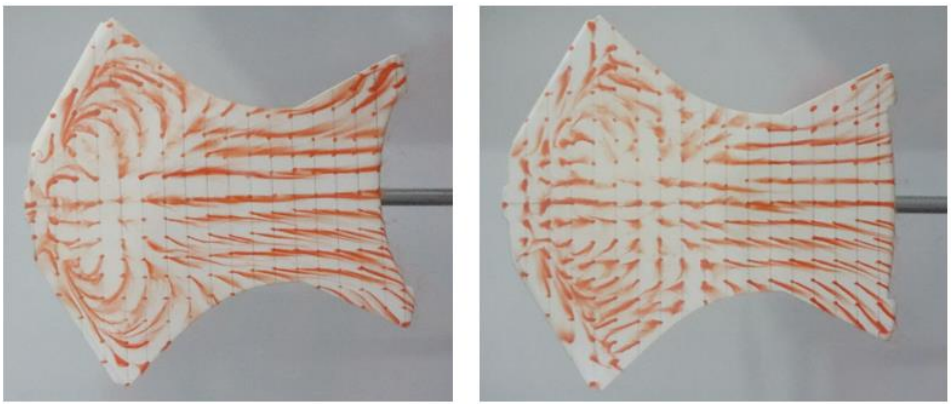

α = 15°

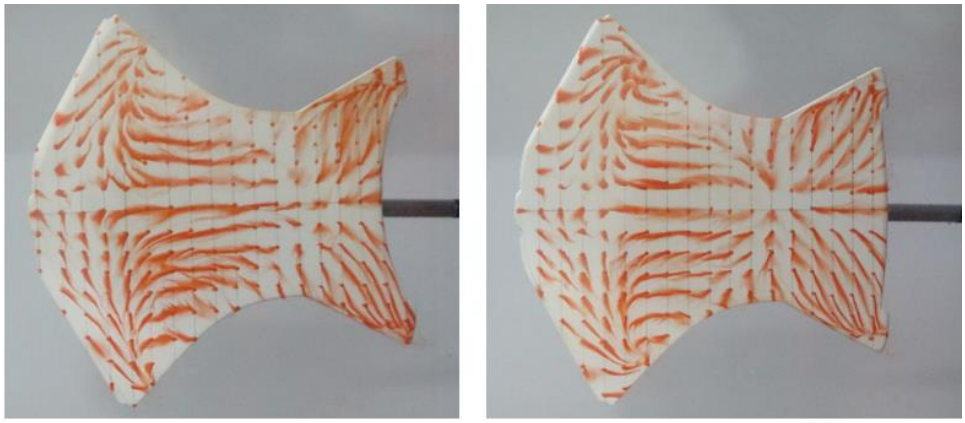

α = 25°

Figure 37. GUS legs 1 (left) and legs 2 (right) during red dot method test at different AOA.

With different design models (GUS Legs 1 and GUS Legs 2) the only difference is that the flow changes direction about 2 cm before the trailing edge for different leg wing designs, while the vortex flow and the reversed flow remains the same. Therefore, the flow reversal and the vortex flow remains the same with different design models.

4.4. Change of AOA effect

Due to previous observation of the flow during the ink flow method test over the GUS design models at different angles of attack, little relevant information was shown regarding our objectives. Therefore, in this section we don't analyze the GUS models using ink flow method.

Original models

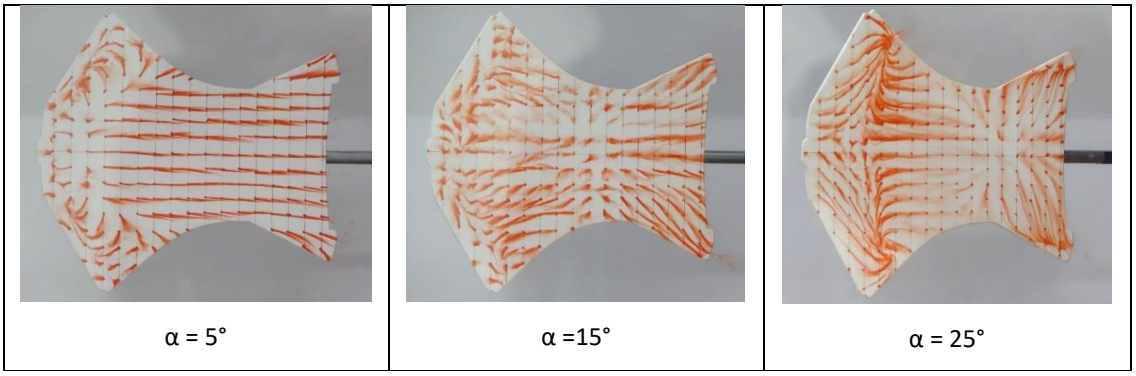

Figure 38. GUS original model during red dot method test at different AOA.

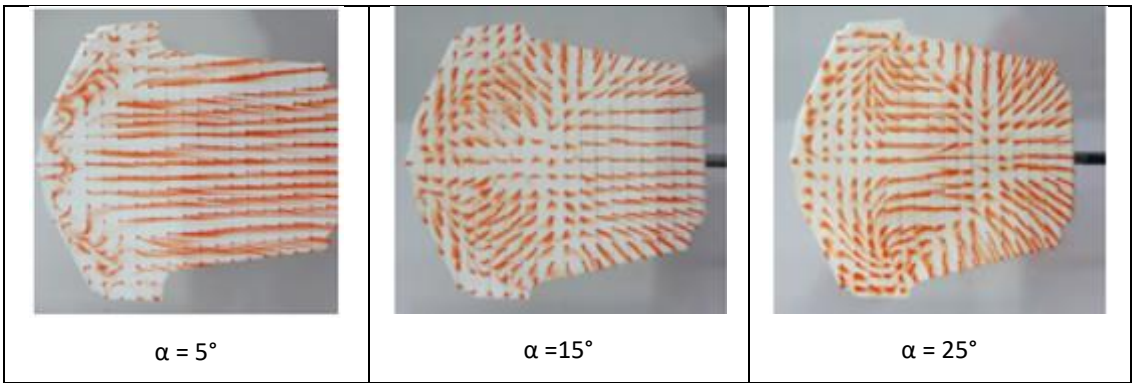

Figure 39. Aura original model during red dot method test at different AOA.

Arms 1 models

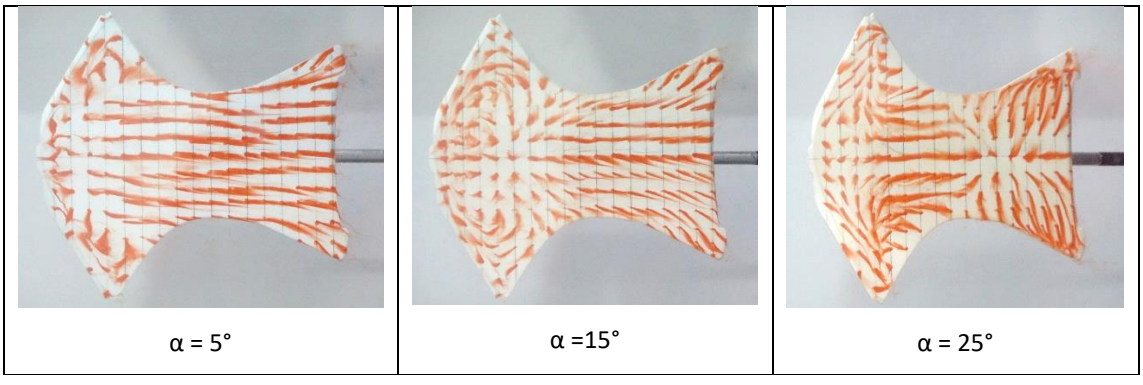

Figure 40. GUS arms 1 model during red dot method test at different AOA.

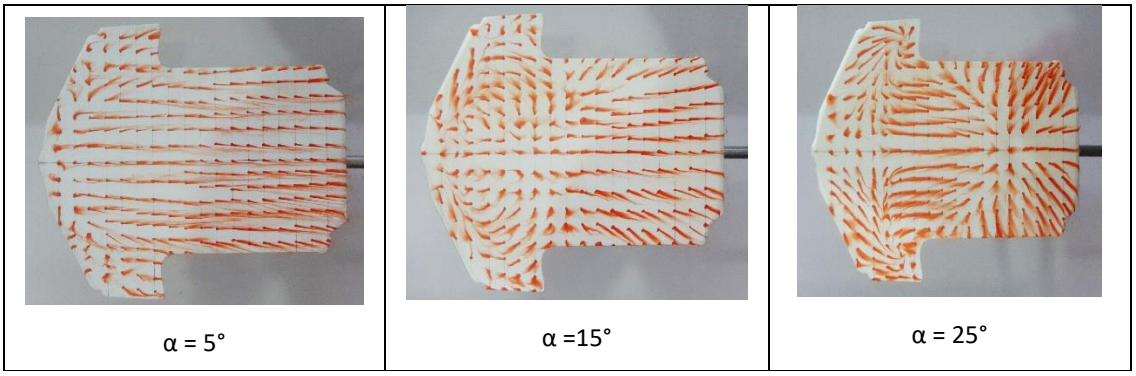

α = 5° | α =15° | α = 25°

Figure 41. Aura arms 1 model during red dot method test at different AOA.

Arms 2 model

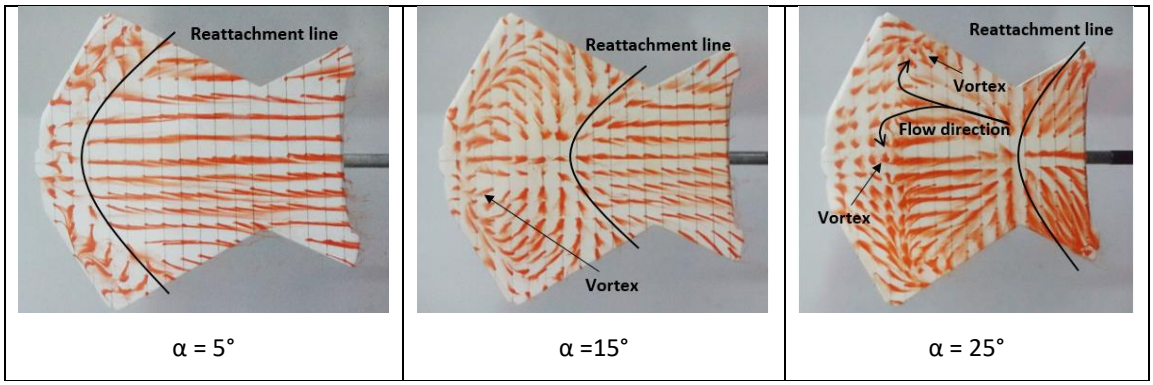

α = 5° | α =15° | α = 25°

Figure 42. GUS arms 2 model during red dot method test at different AOA.

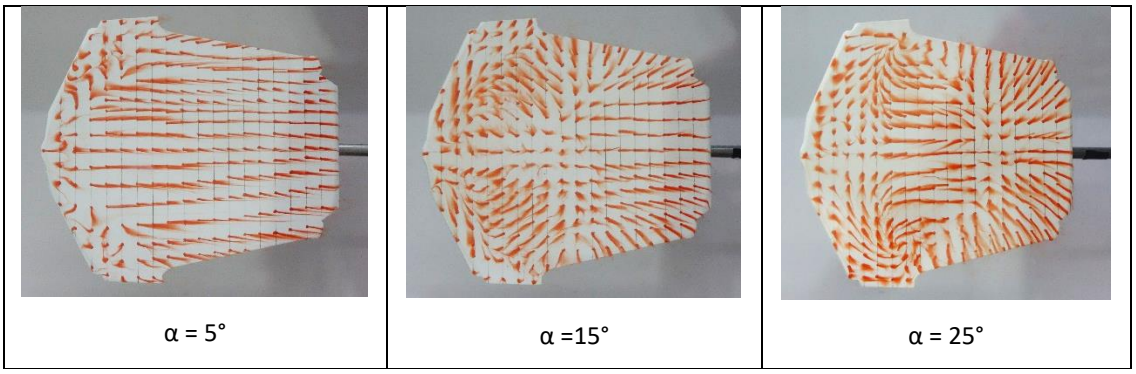

α = 5° | α =15° | α = 25°

Figure 43. Aura arms 2 model during red dot method test at different AOA.

Legs 1 model

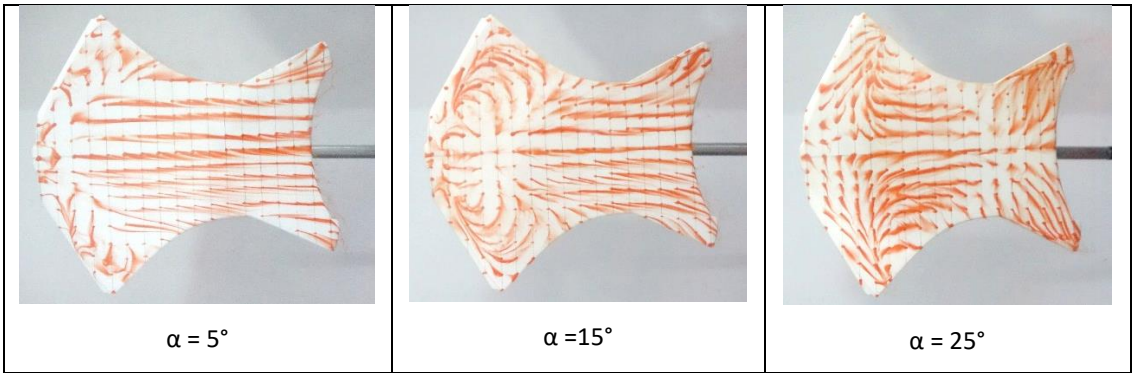

Figure 44. GUS legs 1 model during red dot method test at different AOA.

Legs 2 model

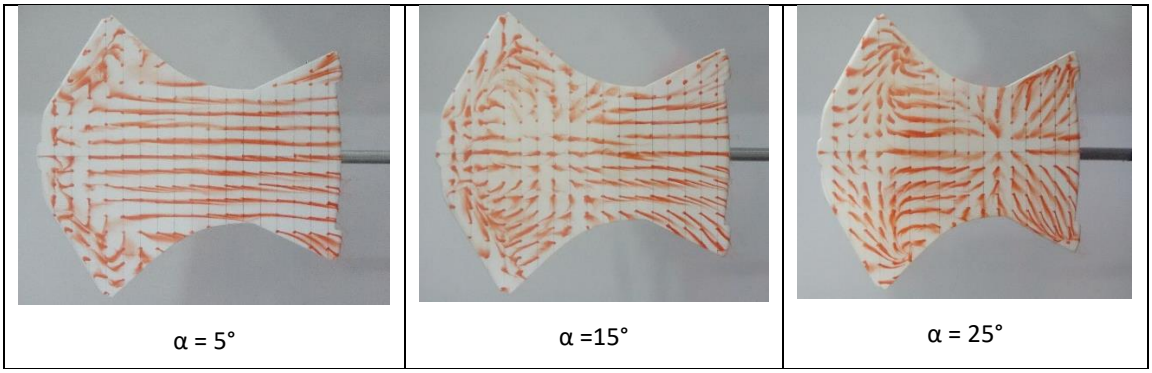

Figure 45. GUS legs 1 model during red dot method test at different AOA.

GUS models discussion

At 5° angle of attack, the separation line for all models is located at 2.5cm from the leading edge and shows a similar parabolic shape as the AURA models at this same angle. It can also be seen vortex instability appearing above the leading edge of the arm's wings that is generated by the flow flowing past the leading edge into the center of the model. After the separation point, the flow uniformly flows parallel to the freestream velocity.

As angle of attack is increased in steady flow up to a range between 5 to 15°, the separation line gradually progresses forward (toward the LE) and at varying distance for each model. The reason why this happens is because the GUS model contains two leading and trailing edges, for both arms and legs.

What happens with the GUS model when the angle of attack gets increased to $25°$, is that the reattachment line is shifted slightly after the start of the leading edge of the leg of the models at 12.5 cm away from the arms leading edge, as seen in figure 42. The geometrical shape doesn't appear to have great influence on the flow behavior for the GUS model. These flow phenomena can be seen in all five GUS models.

AURA models discussion

It is easily observed that models within the $5°$ angle of attack have very similar flow pattern on their structures. This can be appreciated as the separation line for all three Aura models, original (figure 39), arms 1 (figure 41) and arms 2 (figure 43), are within 3 cm from the leading edge of the models. The reason why this parabolic separation line on the AURA model is in the proximities of the leading edge is because AURA models only have one leading edge; in contrast to the beginner GUS model, which has two leading edges.

As the angle of attack increases from $5°$ to $15°$, the separation line moves about 5 cm downstream, this is about 8 cm away from the leading edge, and gets deflected (it acts on the negative direction), as seen in figure 41, therefore generating a vortex acting counterclockwise, due to the interaction of this flow with the freestream, flowing from the leading edge of the wings in a positive direction. Despite the models having different arm structure, at an angle of attack of $15°$, they all share a similar vortex pattern.

When the angle of attack of the models is at $25°$, the separation line is at 14cm apart from the leading edge of all models, despite them having different arm structure. The radius of this parabolic separation curve (in the negative direction) has decreased due to the increased pressure difference on the leading edge of the wing. The direction of the vortices has also changed, from flowing into the middle of the surface to flowing towards the side edges of the arm wings.

The flow phenomena of the AURA models are similar at each angle of attack regardless of their arm structure. They all behave in similar manner, shifting the flow separation line as proportionally as the angle of attack is increased, and generating good looking vortex geometries at the wings. The reason why there are not much flow geometric variations in the models is partly because they all share a similar rectangular shape, and the modification of wing structures are small compared to the area of the model.

4.5. PIV test results

Here the flow field over the wingsuit models showing the magnitude vectors obtained using PIV View 2 and Tecplot software are discussed. Three different planes were selected as shown below, in figure 46:

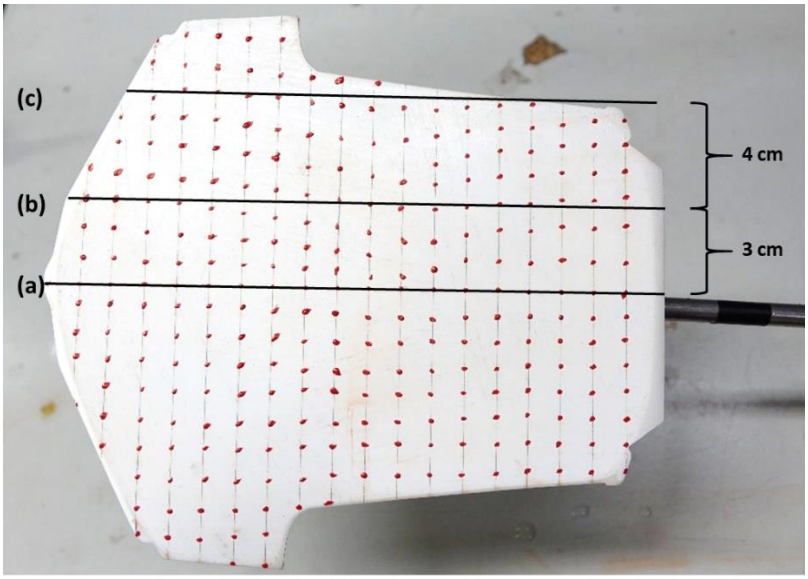

Figure 46. Plane (a), (b) and (c) projected in the AURA model.

(a) Plane of laser sheet at the centerline

(b) Plane of laser sheet 3 cm away from the centerline

(c) Plane of laser sheet 7 cm away from the centerline

The models tested on the PIV are GUS arms 2 and AURA arms 2 both at $\alpha = 15°$, which were selected after obtaining the results of previous test methods, and their respective results are shown below.

GUS Arms 2

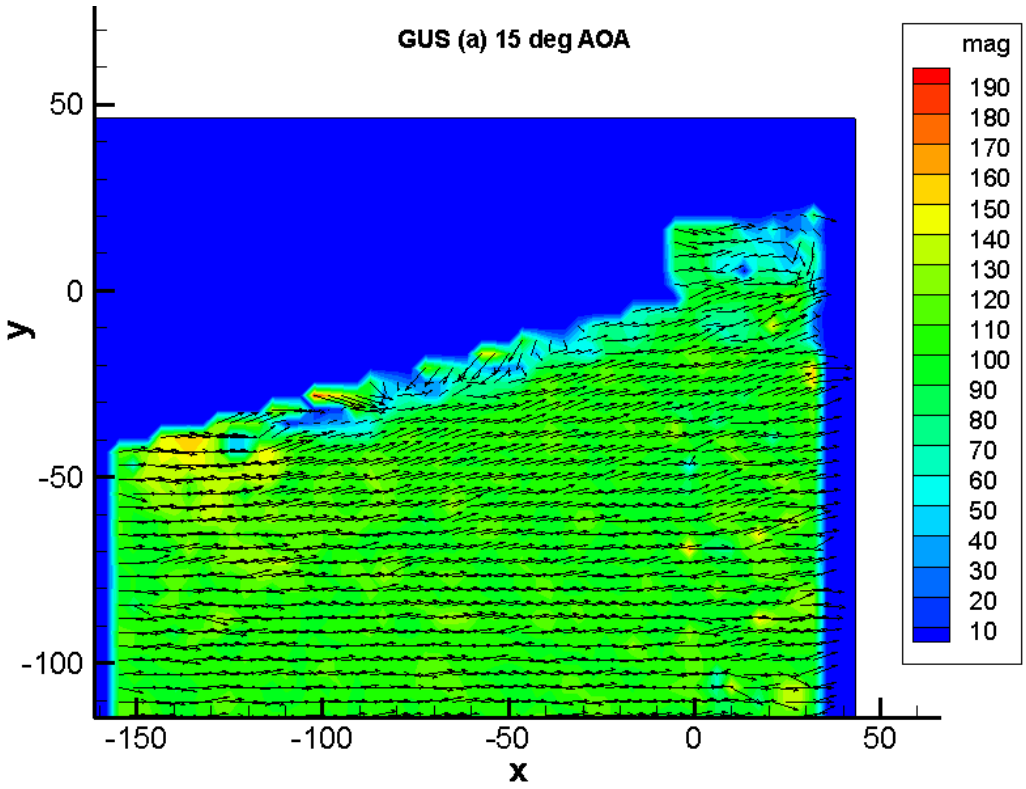

Figure 47. Velocity field of GUS arms 2 design at plane (a) at $\alpha = 15°$.

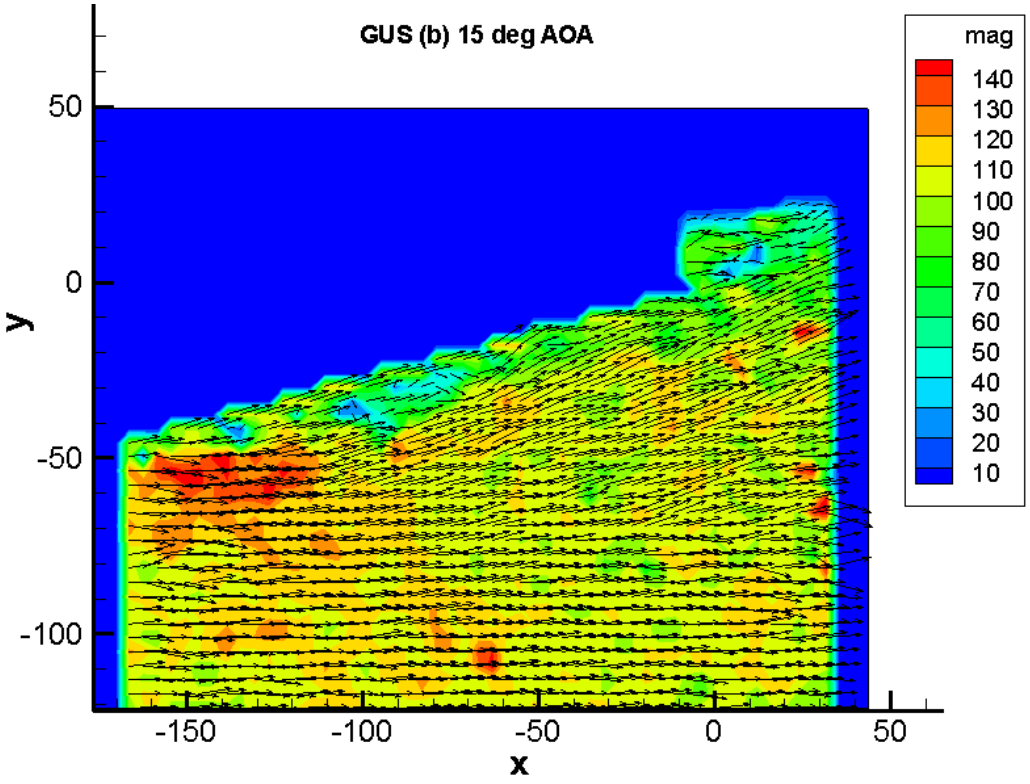

Figure 48. Velocity field of GUS arms 2 design at plane (b) at $\alpha = 15°$.

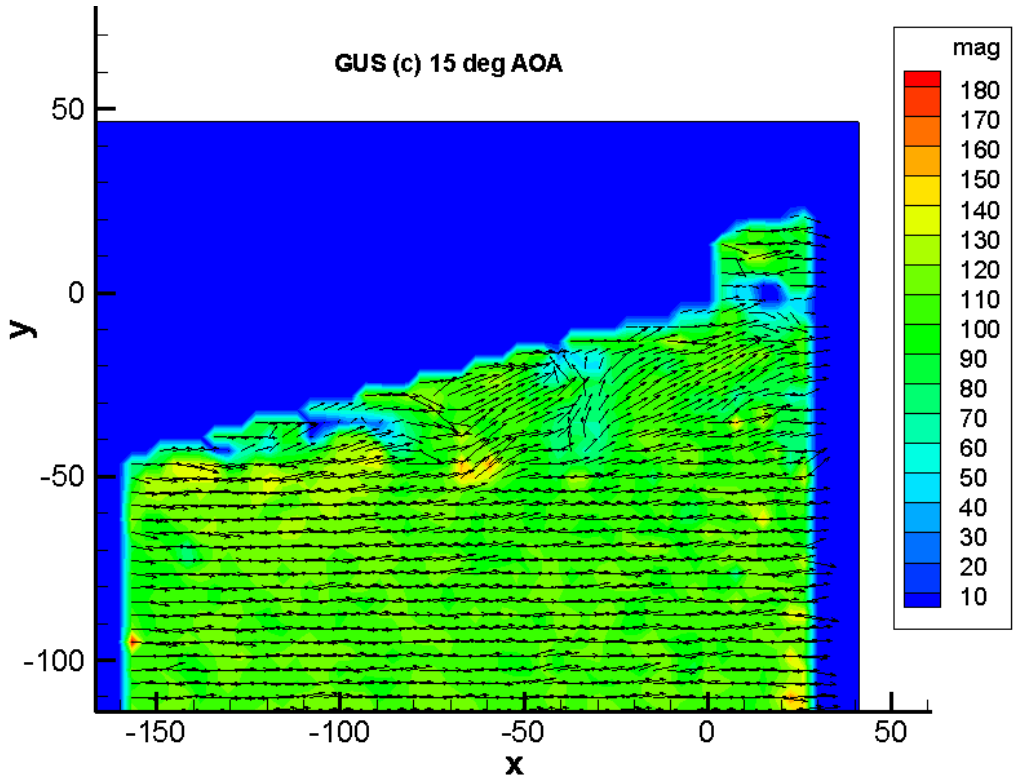

Figure 49. Velocity field of GUS arms 2 design at plane (c) at $\alpha = 15°$.

AURA Arms 2

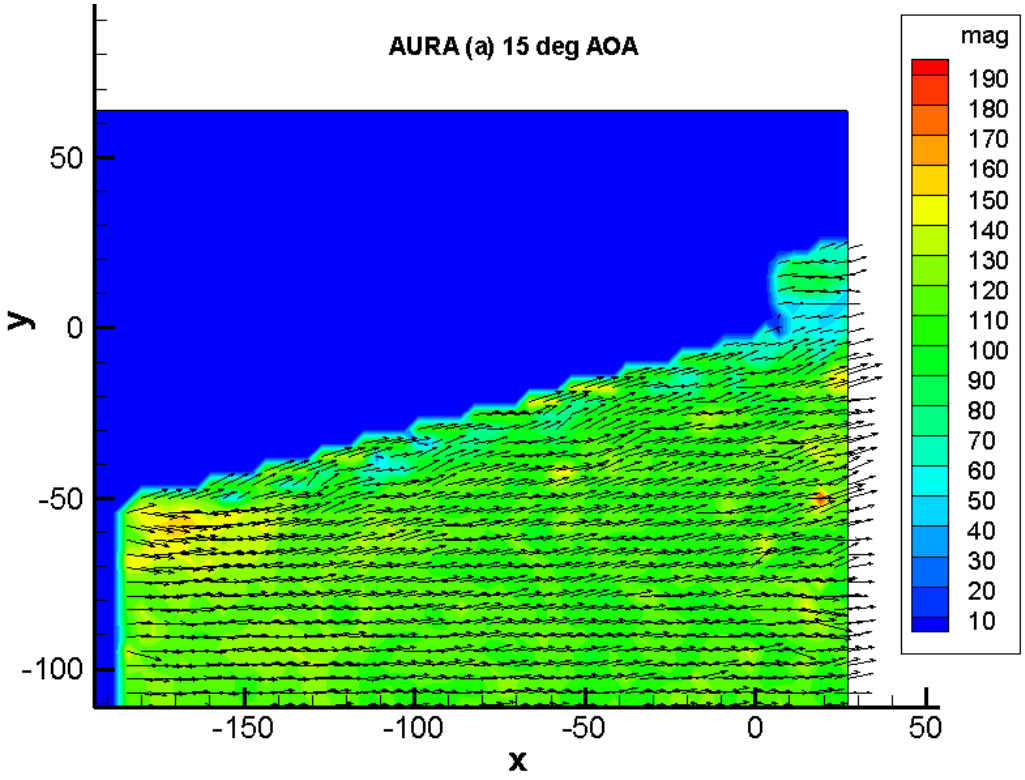

Figure 50. Velocity field of AURA arms 2 design at plane (a) at $\alpha = 15°$.

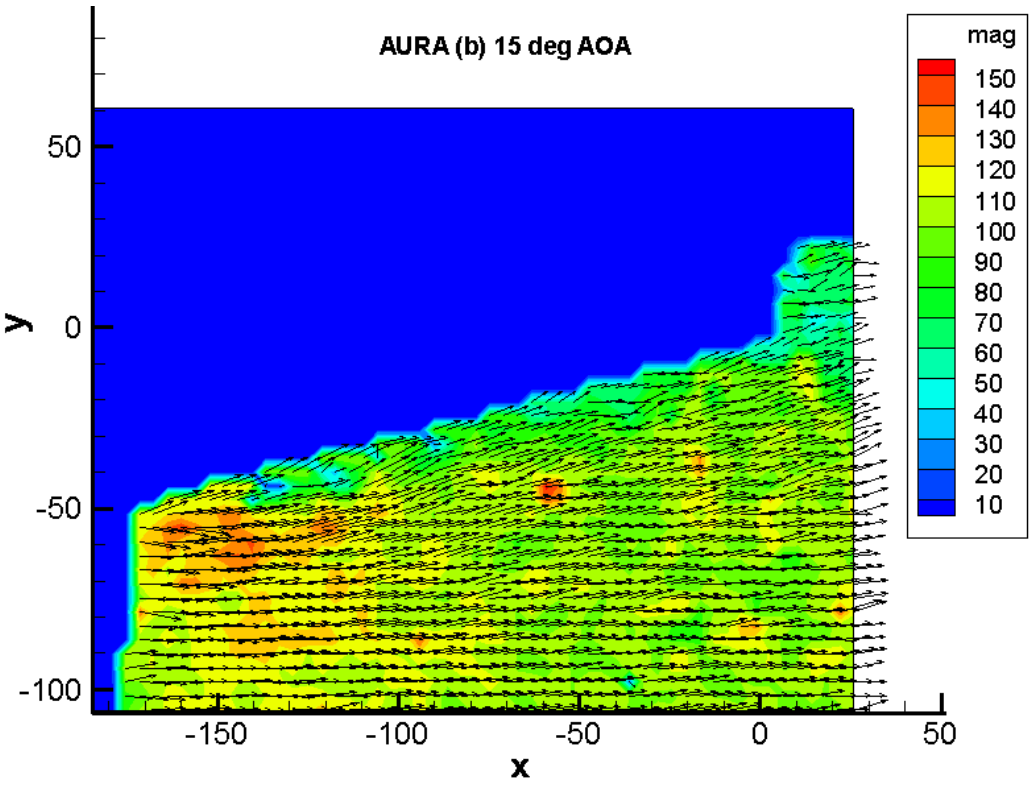

Figure 51. Velocity field of AURA arms 2 design at plane (b) at $\alpha = 15°$.

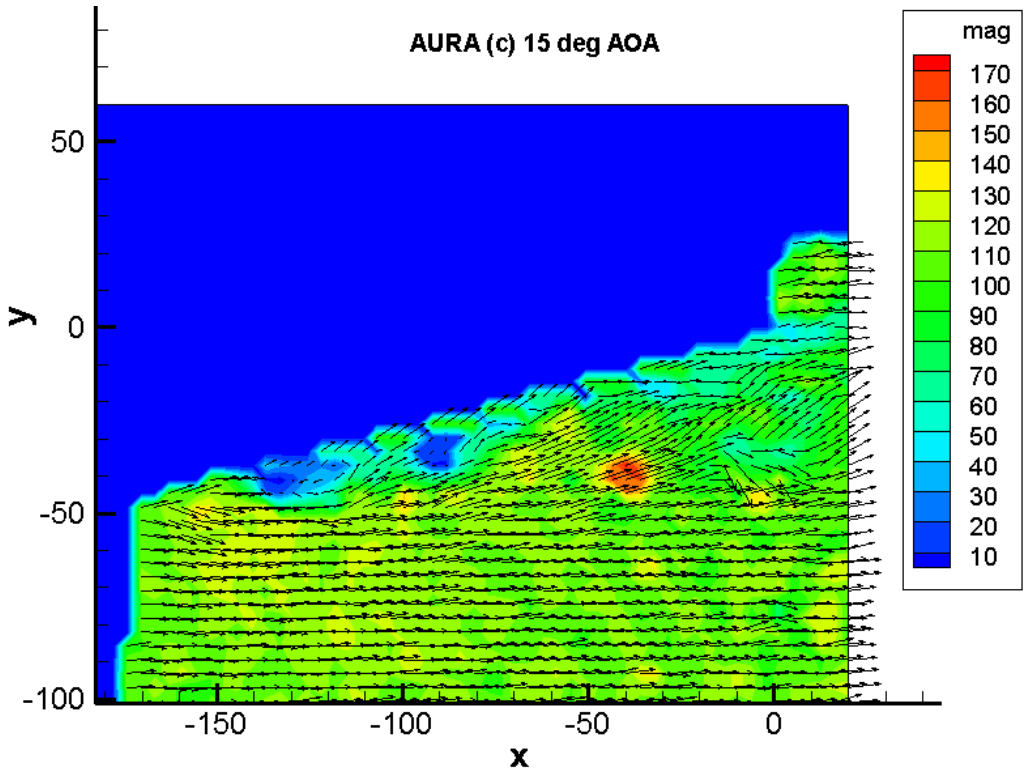

Figure 52. Velocity field of AURA arms 2 design at plane (c) at $\alpha = 15°$.

The magnitude vectors acting on the upper surface of the wingsuit models can be seen in the graphs shown above. The units are given in mm/s.

The plane (a) for both designs (figures 47 and 50) show a steady flow field having a magnitude of about 90 mm/s, shown in green color. This match with the water flow velocity used during the test which was V = 89 mm/s.

For plane (b) (figures 48 and 51), they show stronger magnitude vectors near the leading edge for both GUS Arms 2 and AURA Arms 2 models. The velocity of the vectors increases significantly near the leading edge for both GUS and AURA models to about 130 to 140 mm/s, as shown in red and orange color. Also, a more obvious change in flow direction can be seen near the surface of the models.

For plane (c) (figure 49 and 52), the magnitude of the velocity is lower than that seen in plane (b), having a maximum velocity of approximately V = 140 mm/s. In addition, the flow near the surface shows a reversal in flow direction, producing some vortices. This is because the laser sheet cuts the trailing edge of the arm wings, creating a more complex flow field, as it can be seen on both graphs.

These results are in accordance with those obtained from the red dot method. They prove that the reattachment lines that were visualized during the red dot method occur at the location obtained. In addition, the graphs also prove that the flow's lifting components are mostly concentrated nearer to the leading edge, at the arm wings.

5. Conclusion

In this study we conducted water tunnel test using three different methods, red dot method, ink flow method, and PIV test, to investigate the general aerodynamics of a wingsuit, more specifically the flow on and near the surface by using different approaches as mentioned along this report. It can be seen from this study that there were more vortices concentrated at the region of the arm wings, which in turn induces more lift. This happened for both designs and was more notorious at higher angles of attack, and further away from the centerline of the models.

Regarding the performance, the GUS model is more stable due to the smaller surface area. In addition, it has two leading and two trailing edges, it causes more complex flow near its surface which in turns creates higher drag and lower velocity. On the other hand, the AURA

design is less stable due to the larger area. Also, due to the more stable and steady flow field near the surface, it gives less drag which in turn allows the wingsuit to fly at higher velocities. Therefore, the GUS models are suitable for beginner pilots, while the AURA models for experienced pilots.

The results of this study is important for us, because we gained knowledge and experience regarding the phenomena and characteristics involved in a fluid flow and the different methods used to obtain them. In addition, this study could be of benefit for the wingsuit community and/or anyone interested in this topic for further study.

6. References

[1] Ferguson, Maria E. "Flying without Dying: The Future of Wingsuit Design". (2016). Technical Writing Final Project.

[2] Berry, Michael, Jonathan Las Fargeas, and Kim B. Blair. “Wind Tunnel Testing of a Novel Wingsuit Design.” Procedia Engineering 2, no. 2.

[3] Sestak, Timothy Allen. (2015). “Development of a Robust Wind Tunnel Balance for Wingsuit Aerodynamic Testing”.

[4] Stephanopoulos, Kimon; Levy, Ben; and Rabadan, Ignacio Jr., "Designing a High-Lift Performance Wingsuit" (2015). Mechanical Engineering Design Project Class. Paper 26.

[5] Robson, G., & D’Andrea, R. (2010). “Longitudinal Stability Analysis of a Jet-Powered Wingsuit”. AIAA Atmospheric Flight Mechanics Conference.

[6] Sestak, Timothy A. (2017). "The Effect of Surface Materials and Morphology on Wingsuit Aerodynamics". Dissertations and Theses.

[7] Maria E. Ferguson and Ramesh K. Agarwal. (2018). “Design and Computational Fluid Dynamics Analysis of an Idealized Modern Wingsuit”. AIAA SciTech Forum.

[8] Nazanin Ansari, Sybille Krzywinski and Jochen Fröhlich. (2018). “Towards a Combined CAD and CFD Development Process of a Wingsuit”.

[9] Xiaomo, Z. (2016). “Flight Dynamics Simulation and Stability Control of Wingsuits”.

[10] Leon, S. and Morris, M. (2010). “Force Balance Design for Educational Wind Tunnels”.

[11] Weed, W. S. (2003, June 18). "The Flight of the Bird Men". Popular Science (Online).

[12] Squirrel Wingsuits, LLC. (2018).

[13] USPA United States Parachute Association. (2017).

[14] Abrams, M. (2003, May 26). “The birdman of DeLand”. Forbes (Online).

[15] Higgins, M. (2014). “Bird Dream: Adventures at the Extremes of Human Flight”. New York: Penguin Group Inc.

[16] Higgins, M. (2015, August 30). “The grandpa who helps men fly”. Outside Online (Online).

[17] Panero, J., & Zelnik, M. (1979). “Human dimension and interior space: a source book of design reference standards”. New York: Watson-Guptill.

[18] Panero, J., & Zelnik, M. (2014). “Human dimension and interior space: a source book of design reference standards”. New York: Watson-Guptill.

[19] Chen H., Pan C., Wang J. J. (2013) “Effects of sinusoidal leading edge on delta wing performance and mechanism”. Sci China Tech Sci.